PLOS Computational Biology

The physiological variability of channel density in hippocampal CA1 pyramidal cells and interneurons explored using a unified data-driven modeling workflow

--Manuscript Draft--

Manuscript Number:	PCOMPBIOL-D-18-00424R1
Full Title:	The physiological variability of channel density in hippocampal CA1 pyramidal cells and interneurons explored using a unified data-driven modeling workflow
Short Title:	Channel density variability among CA1 neurons
Article Type:	Research Article
Keywords:	Computational neuroscience, Hippocampus, CA1 neurons, Ionic Channels, Degeneracy
Corresponding Author:	Rosanna Migliore Consiglio Nazionale delle Ricerche Palermo, ITALY
Corresponding Author Secondary Information:	
Corresponding Author's Institution:	Consiglio Nazionale delle Ricerche
Corresponding Author's Secondary Institution:	
First Author:	Rosanna Migliore
First Author Secondary Information:	
Order of Authors:	Rosanna Migliore
	Carmen Alina Lupascu
	Luca Leonardo Bologna
	Armando Romani
	Jean-Denis Courcol
	Stefano Antonel
	Werner A.H. Van Geit
	Alex M. Thomson
	Audrey Mercer
	Sigrun Lange
	Joanne Falck
	Christian Andreas Rössert
	Ying Shi
	Olivier Hagens
	Maurizio Pezzoli
	Tamás F. Freund
	Eilif Benjamin Muller
	Szabolcs Kali
	Felix Schürmann
	Henry Markram
	Michele Migliore

Order of Authors Secondary Information:	
Abstract:	Every neuron is part of a network, exerting its function by transforming multiple spatiotemporal synaptic input patterns into a single spiking output. This function is specified by the particular shape and passive electrical properties of the neuronal membrane, and the composition and spatial distribution of ion channels across its processes. For a variety of physiological or pathological reasons, the intrinsic input/output function may change during a neuron's lifetime. This process results in high variability in the peak specific conductance of ion channels in individual neurons. The mechanisms responsible for this variability are not well understood, although there are clear indications from experiment and modeling that degeneracy and correlation among multiple channels may be involved. Here, we studied this issue in biophysical models of hippocampal CA1 pyramidal neurons and interneurons. Using a unified data-driven simulation workflow and starting from a set of experimental recordings and morphological reconstructions obtained from rats, we built and analyzed several ensembles of morphologically and biophysically accurate single cell models with intrinsic electrophysiological properties consistent with experimental findings. The results suggest that the set of conductances expressed in any given hippocampal neuron may be considered as belonging to two groups: one subset is responsible for the major characteristics of the firing behavior in each population and the other responsible for a robust degeneracy. Analysis of the model neurons suggested several experimentally testable predictions related to the combination and relative proportion of the different conductances that should be expressed on the membrane of different types of neurons for them to fulfill their role in the hippocampus circuitry.
Suggested Reviewers:	Sergio Solinas, PhD Universita degli Studi di Sassari smgsolinas@gmail.com
	Giorgio Ascoli George Mason University ascoli@gmu.edu
	William W Lytton SUNY DOWNSTATE MEDICAL CENTER bill.lytton@downstate.edu
	Nicholas Carnevale Senior Research Scientist, Yale University School of Medicine ted.carnevale@yale.edu
Opposed Reviewers:	
Additional Information:	
Question	**Response**
Financial Disclosure Please describe all sources of funding that have supported your work. **This information is required for submission and will be published with your article, should it be accepted.** A complete funding statement should do the following: 1. Include grant numbers and the URLs of any funder's website. Use the full name, not acronyms, of funding institutions, and use initials to identify authors who received the funding. 2. **Describe the role** of any sponsors or funders in the study design, data	The experimental data used in this study resulted from the work of many years that was supported by the Wellcome Trust (1994- 2000), the Medical Research Council (1995–2008), Sandoz/Novartis Pharma (1994–2008) and Glaxo Smith Kline (2004-2008). This project has received funding from the European Union's Horizon 2020 research and innovation programme under grant agreement No 720270.

collection and analysis, decision to publish, or preparation of the manuscript. If the funders had **no role** in any of the above, include this sentence at the end of your statement: "*The funders had no role in study design, data collection and analysis, decision to publish, or preparation of the manuscript.*" However, if the study was **unfunded**, please provide a statement that clearly indicates this, for example: "*The author(s) received no specific funding for this work.*" * typeset	
Competing Interests You are responsible for recognizing and disclosing on behalf of all authors any competing interest that could be perceived to bias their work, acknowledging all financial support and any other relevant financial or non-financial competing interests. Do any authors of this manuscript have competing interests (as described in the PLOS Policy on Declaration and Evaluation of Competing Interests)? **If yes**, please provide details about any and all competing interests in the box below. Your response should begin with this statement: *I have read the journal's policy and the authors of this manuscript have the following competing interests:* **If no** authors have any competing interests to declare, please enter this	The authors have declared that no competing interests exist

statement in the box: "*The authors have declared that no competing interests exist.*" * typeset	
Data Availability PLOS journals require authors to make all data underlying the findings described in their manuscript fully available, without restriction and from the time of publication, with only rare exceptions to address legal and ethical concerns (see the PLOS Data Policy and FAQ for further details). When submitting a manuscript, authors must provide a Data Availability Statement that describes where the data underlying their manuscript can be found. Your answers to the following constitute your statement about data availability and will be included with the article in the event of publication. **Please note that simply stating 'data available on request from the author' is not acceptable.** ***If, however, your data are only available upon request from the author(s), you must answer "No" to the first question below, and explain your exceptional situation in the text box provided.*** Do the authors confirm that all data underlying the findings described in their manuscript are fully available without restriction?	Yes - all data are fully available without restriction
Please describe where your data may be found, writing in full sentences. **Your answers should be entered into the box below and will be published in the form you provide them, if your manuscript is accepted.** If you are copying our sample text below, please ensure you replace any instances of XXX with the appropriate details. • If your data are all contained within the	Data are from the R. Migliore et al. study whose authors may be contacted at rosanna.migliore@cnr.it.

paper and/or Supporting Information files, please state this in your answer below. For example, “All relevant data are within the paper and its Supporting Information files.” • If your data are held or will be held in a public repository, include URLs, accession numbers or DOIs. For example, “All XXX files are available from the XXX database (accession number(s) XXX, XXX)." If this information will only be available after acceptance, please indicate this by ticking the box below. • If neither of these applies but you are able to provide details of access elsewhere, with or without limitations, please do so in the box below. For example: “Data are available from the XXX Institutional Data Access / Ethics Committee for researchers who meet the criteria for access to confidential data.” “Data are from the XXX study whose authors may be contacted at XXX.” * typeset	
Additional data availability information:	

Dear Editor,

in this paper we investigate the channel density variability among hippocampal CA1 neurons. The mechanisms responsible for this variability are not well understood, although there are clear indications from experiment and modeling that degeneracy and correlation among multiple channels may be involved. In this work, using a unified data-driven simulation workflow we study this issue, for the first time, in data-driven single cell models of hippocampal CA1 pyramidal neurons and interneurons with intrinsic electrophysiological properties consistent with experimental findings. The results suggest that the set of conductances expressed in any given hippocampal CA1 neuron may be considered as belonging to two groups: one subset is responsible for the major characteristics of the firing behavior in each population and the other is responsible for a robust degeneracy. An analysis of the models suggests several experimentally testable predictions related to the combination and relative proportion of the different conductances that should be expressed on the membrane of different types of neurons for them to fulfill their role in the hippocampus circuitry. We think that these results can be of great interest to the broad community of readers of this journal.

Responses to Reviewers

We thank the reviewers for the constructive comments. We have taken into account all points by revising the text as explained below. A new figure (#7) has been added.

Reply to Reviewer: 1

Reviewer #1: General comments:

Excellent paper/study showing parameter degeneracy in pyramidal and interneurons of the hippocampus that will be of wide interest to the readers of PCBIO. Availability of tools/software/data further strengthen the paper. Authors find that there are two subsets of parameters, one which contributes to firing, other which enables degeneracy. Modeling/data is state-of-the-art. However, some of the arguments could use clarification, e.g. the definition of degeneracy, and how it realtes to stability is often not clearly specified, particularly early on in the paper. The authors could also more extensively explore how the geometry of the neurons relates to degeneracy - for example, if they are optimizing a population of models with different geometries, is there a way to first quantify the geometry (e.g. dendrite properties), and then to predict what the channel conductance levels would be? This type of distinguishing between the role of geometry and channel densities would allow better understanding of where a neuron's dynamics come from - so if the authors can add some analysis/discussion of this, it would improve clarity/interestingness of the paper. Further framing of discussion would help as well (see detailed comments below).

Detailed comments:

- *Line 42: "Both within and between neurons, individual ion channel peak conductance is highly variable." What does it mean conductance variability within a single neuron? Variability across time or across different locations within the neuron at the same time? Please clarify which meaning you intended*
  The sentence has been revised as: “The peak conductance of many ion channel types measured in any given animal is highly variable across neurons, both within and between neurons populations”. We hope this clarifies that we intended variability across individual neurons from the same population in the same animal.

- *line 52: "robust degeneracy" - what is the value of robust degeneracy?*
  the sentence has been revised, and it now reads “...and the other more involved with degeneracy”

- *line 66: "is the high variability for the current generated by specific ion channels in individual neurons, " - clarify again whether the variability refers to variability across time? Should the authors replace "by specific ion channels" with "by specific types of ion channels"?*
  The sentence has been revised, and it should now be clearer that we meant “the high variability for the current generated by specific types of ion channels measured across individual neurons,”

- *lines 69-71: If degeneracy is a way for a neuron to maintain the same function through different means, then how is it tunable? Wouldn't tuning the function by definition change the function? The definitions need to be clarified. Correlation in the function of a variety of conductances - this needs to be more clearly explained as well; what is the value of having correlated conductance values?*
  Several sentences in this paragraph have been revised/rewritten, to take also into account a comment by the other reviewer on the same issue. We hope that this point is now clearer.

- *line 77: "biochemical processes" - which processes? Please spell out a few examples by name*
  "...such as activation of protein kinase A and C, or Ca/calmodulin dependent kinase II" has been added to the sentence.

- *88-90: how can you cleanly separate out the two sets of ion channels - if some channels are responsible for firing activity, wouldn't they influence the ability of the other channels to contribute degeneracy? For example, fast na/k channels will contribute to firing but even at rest they will have some non-zero conductance. Altering their densities slightly might require other channel densities to shift to maintain the activity. so the na/k channels will contribute to both firing properties as well as the exact mechanism of degeneracy. The whole argument needs to be clarified.*
  The sentence has been deleted and a new one has been added to clarify this point.

- *97: superposed -> superimposed*
  DONE

- *Figure 1 caption: " 990803, oh140807_A0_idJ," <- what are these? Names/identifiers of individual neurons? Please clarify*
  Correct. These names identify the different cell reconstructions. The caption of figure 1 has been slightly revised.

- *line 120: briefly define "continuous accomodating cells (cAC)." vs cNAC; e.g. firing rate changes during the current injection vs. ~constant firing rate*

  We added two shorts sentences to clarify that firing patterns with "an increasing inter-spike-interval (ISI)" are classified as cAC while "traces, whose firing rate is constant," as cNAC.

- *line 140: "classified as classic adapting cells (cAC);" - previously cAC was defined as continuous accomodating cells. Use consistent terminology or explain that they're identical.*
  We have revised the text to consistently use "continuous accommodating", "continuous non-accommodating", and "bursting accommodating" as in Markram et al., Cell 2015 [18].

- *figure 3 - please show the absolute membrane potential so readers can see the resting membrane potential level and whether it differs from experiments shown in figure 2.*
  Following the referee suggestion, we have modified both fig 3 and fig 2 so the readers can compare the resting membrane potential of the experimental traces and the simulated ones.

- *lines 145 - 147: can the authors clarify if there are a set of models produced from every set of voltage traces and individual morphology used in the optimization procedure? Or a single model from the set of voltage traces + morphology? Or is the procedure explicitly fitting a whole population at once rather than fitting individuals?*
  The sentences relative to this comment have been revised to hopefully make it more clear that: "The whole set of somatic voltage traces obtained from all cells classified as belonging to any given e-type, were used to extract a set of electrophysiological features, one for each e-type (see S1-S4 Tables and *Methods*). All the pyramidal cell morphologies were used to implement *cAC* models, whereas interneuron morphologies were used to obtain *cAC*, *cNAC*, and *bAC* models following the known firing behavior of each type of morphology (see legend of Fig 1 and S5 Table). Features and morphologies were then used to obtain a set of optimized models for each e-type, by a heuristic parameter optimization process employing multi-objective genetic algorithms."

The fit was thus relative to a whole population, not to individual cells.

- *line 164: "havingreached" -> having reached* DONE
- *figure 4 : for the voltage traces show the absolute levels so readers can infer the RMP and whether model RMPs are similar the shapes of the interspike intervals look very different; is ISI voltage one of the objective functions? if so, why do they differ so much?*
  Fig.4 has been revised by adding axes to both model and exp traces.

  The voltage between spikes was not among the optimized features (see Supplementary Tables S1-S4). Its accurate reproduction would require to also optimize channel kinetics, and this was outside the scope of this work.

- *lines 228-229: "The optimization process generates many of these models (termed "individuals"), because of ion channel degeneracy [2]." can the authors explain if it is only due to degeneracy or also because there are different morphologies used for a fixed set of voltage traces? in either case, the authors should clarify if they see the same morphology producing the same response with different channel densities.*
  A sentence has been added to clarify that the 10 best individuals for each optimization run were obtained from the same morphology with different channel densities.

  A new figure (fig. 7) has been added to show that degeneracy can also be obtained using different morphologies equipped with identical peak channels conductance. A deeper analysis of this issue however was not further considered in this work.

- *line 240: "highlighted in red" ; mention that the text label is highlighted in red, confusing since red colors are used in the figure's heatmap*
  The sentence "using a red label in the y axis" has been added to clarify this point.

- *discussion - 343 - the discussion would be enhanced by comparing to not only somatograstric ganglion cell parameter degeneracy but to some other recent papers that showed similar results with regards to parameter degeneracy in layer 5 cortical pyramidal neurons and in motor cortex network levels:*
  J Neurophysiol 117:148-162, 2017
  Front Pharmacol 7:157, 2016
  The relevant paragraph has been extended to include these papers.

- *Lines 369-376: How does the optimization approach differ from other recent modeling studies such as those used in Nature Communications 9 (1), 710, 2018*
  and J Neurophysiol 117:148-162, 2017?
  A new paragraph has been added to the Methods section, to compare the approaches used in these papers with that used in this work.

Reply to Reviewer: 2

Reviewer #2: *The manuscript describes an interesting approach to the study of cellular mechanisms that might give rise to degeneracy phenomena in vertebrate neurons. For the most part its methods and results are clearly spelled out and are reasonable, but some issues need to be resolved.*

- *Figure 1--This is cosmetic, but important. The interneurons in the bottom half of the figure are very difficult to see and are likely to disappear in a published article's crude bitmap. Converting the background, or even the entire image, to a negative might make them more salient.*
  Fig.1 has been revised by using a negative background

- *line 47-48*
  "we systematically generated a range of morphologically and biophysically accurate single cell models" seems an overstatement in light of the actual procedures. The models' morphology came straight from morphometric data obtained under light microscopy (good). However, the biophysical parameters were tuned by an algorithm that involved heuristic adjustments so that model responses to injected currents approximate multiple experimental objectives well enough for the sum of standard deviations over all objectives to be less than some (unspecified) value. What is that value? For any objective a standard deviation < 2 was considered acceptable, and a model cell "with an acceptable score for all objectives" was considered "plausible" (lines 152-157). That's not a close match to what readers might regard as the ordinary meaning of "accurate."
  We apologize for the confusion. The term "biophysically accurate" in the Author Summary refers to the type and distribution of ion channel kinetics. It is a widely used way to indicate models in which the active properties of a cell are directly based on experimental data, as opposed to models using artificial or simplified conductances. The sentence has been revised, trying to avoid any possible confusion with the optimization process.

  In regards to the point on the acceptable individual, the paragraph has been rewritten in such a way to make it clear that: "The final choice to accept an individual as a plausible representation of a given e-type, was based on the error obtained for each objective. An individual with a sd<2 for all objectives was considered acceptable".

- *lines 69-71*
  "Degeneracy, in particular, is thought to be a fundamental mechanism to allow a neuron to adjust its firing properties in a robust and tunable manner". Degeneracy is no more a mechanism than is stability. Edelman and Gally defined degeneracy as "the ability of elements that are structurally different to perform the same function or yield the same output" (Degeneracy and complexity in biological systems Gerald M. Edelman and Joseph A. Gally PNAS November 20, 2001. 98 (24) 13763-13768). They referred to it as a property of complex biological systems, but not as a mechanism in and of itself. It would be correct to say that "the phenomenon of degeneracy enables the robust and tunable adjustment of a neuron's firing properties."
  We agree with the reviewer. The related sentences have been revised, to take also into account a point raised by the other reviewer on the same issue.

- *lines 165-167*
  Unless I'm completely misinterpreting Fig. 3, it does not show that "in most cases, the associated error . . . was below 2 sd." It shows only the score for an individual model cell.
  The sentence has been revised as: "for most features (n=60 for pyramidal cells and n= 47 for cAC interneurons, see S1-S4 Tables), the associated error was below 2 sd

- *The top two sets of plots of v vs. t in Fig. 3 have a peculiar artifact near the end of current injection, where the traces loop back in time and then decay linearly with time.*
  We thank the reviewer for spotting this problem. We removed the artifacts.

- *line 265*
  Instead of using the oxymoronic phrase "relatively constant," why not just say that some parameters were found to lie in a narrow range?
  Done

- *The radar plots in Fig. 8 don't add much--too many overlapping, zigzagging lines, with no obvious correlations.*
  We would like to keep this figure, because it indeed conveys an immediate, and visually impressive, representation of the lack of correlation among the different conductances, in spite of being able to concur to essentially equivalent electrophysiological properties

- *line 358 "no cell type showed the same set of pairwise correlations" as what?*
  The sentence has been revised as "...no cell type showed conductances with the same set of pairwise correlations."

- *line 372 optimize -> optimizing* DONE

- *388 explanation on -> explanation for* DONE

- *400 and involved -> and is involved* DONE

- *493 run -> running* *explore -> exploring* DONE

The physiological variability of channel density in hippocampal CA1 pyramidal cells and interneurons explored using a unified data-driven modeling workflow.

Rosanna Migliore[1], Carmen A. Lupascu[1], Luca L. Bologna[1], Armando Romani[2], Jean-Denis Courcol[2], Stefano Antonel[2], Werner A.H. Van Geit[2], Alex M. Thomson[4], Audrey Mercer[4], Sigrun Lange[4,5], Joanne Falck[4], Christian A. Rössert[2], Ying Shi [2], Olivier Hagens [6], Pezzoli Maurizio [6], Tamas F. Freund[3,7], Szabolcs Kali[3,7], Eilif B. Muller[2], Felix Schürmann[2], Henry Markram[2], and Michele Migliore[1]

[1] Institute of Biophysics, National Research Council, Palermo, Italy,

[2] Blue Brain Project, École Polytechnique Fédérale de Lausanne, Campus Biotech, Geneva, Switzerland,

[3] Institute of Experimental Medicine, Hungarian Academy of Sciences, Budapest, Hungary,

[4] University College London, United Kingdom,

[5] University of Westminster, London, United Kingdom,

[6] Laboratory of Neural Microcircuitry (LNMC), Brain Mind Institute, EPFL, Lausanne, Switzerland

[7] Faculty of Information Technology and Bionics, Pázmány Péter Catholic University, Budapest, Hungary.

Corresponding author: rosanna.migliore@cnr.it (RM)

Short Title: Channel density variability among CA1 neurons

Abstract

Every neuron is part of a network, exerting its function by transforming multiple spatiotemporal synaptic input patterns into a single spiking output. This function is specified by the particular shape and passive electrical properties of the neuronal membrane, and the composition and spatial distribution of ion channels across its processes. For a variety of physiological or pathological reasons, the intrinsic input/output function may change during a neuron's lifetime. This process results in high variability in the peak specific conductance of ion channels in individual neurons. The mechanisms responsible for this variability are not well understood, although there are clear indications from experiment and modeling that degeneracy and correlation among multiple channels may be involved. Here, we studied this issue in biophysical models of hippocampal CA1 pyramidal neurons and interneurons. Using a unified data-driven simulation workflow and starting from a set of experimental recordings and morphological reconstructions obtained from rats, we built and analyzed several ensembles of morphologically and biophysically accurate single cell models with intrinsic electrophysiological properties consistent with experimental findings. The results suggest that the set of conductances expressed in any given hippocampal neuron may be considered as belonging to two groups: one subset is responsible for the major characteristics of the firing behavior in each population and the other responsible for a robust degeneracy. Analysis of the model neurons suggests several experimentally testable predictions related to the combination and relative proportion of the different conductances that should be expressed on the membrane of different types of neurons for them to fulfill their role in the hippocampus circuitry.

Author Summary

The peak conductance of many ion channel types measured in any given animal is highly variable across neurons, both within and between neuronal populations. The current view is that this occurs because a neuron needs to adapt its intrinsic electrophysiological properties either to maintain the same operative range in the presence of abnormal inputs or to compensate for the effects of pathological conditions. Limited experimental and modeling evidence suggests this might be implemented via the correlation and/or degeneracy in the function of multiple types of conductances. To study this mechanism in hippocampal CA1 neurons and interneurons, we systematically generated a set of morphologically and biophysically accurate models. We then analyzed the ensembles of peak conductance obtained for each model neuron. The results suggest that the set of conductances expressed in the various neuron types may be divided into two groups: one group is responsible for the major characteristics of the firing behavior in each population and the other more involved with degeneracy. These models provide experimentally testable predictions on the combination and relative proportion of the different conductance types that should be present in hippocampal CA1 pyramidal cells and interneurons.

Introduction

Any given neuron in the brain is part of a network, in which it exerts its action by transforming the input it receives into an output. This function is specified by the particular shape and passive electrical properties of the neuronal membrane, the composition and spatial distribution of ion channels across its processes, and the functional properties of the synaptic inputs themselves. During development and during the entire lifetime of a neuron, its input/output function is adapted to realize ongoing refinement of the function of the neuron and circuit, or maintain functional robustness in the face of constant protein turnover or an evolving pathological condition. Such adaptability of individual neurons can be achieved through a myriad of dynamic mechanisms, including structural, intrinsic, and synaptic plasticity. A direct experimental evidence for these mechanisms is the high variability observed for the current generated by specific types of ion channels measured across individual neurons, from either a homogeneous population or different cell populations (e.g. [1]). The mechanisms responsible for this variability are not well understood, although there are clear experimental and modeling indications that correlation and degeneracy among a variety of conductances can be involved [2,3]. The phenomenon of degeneracy allows the possibility, for a complex biological system, to perform the same function using structurally different elements [4]. In the context considered in this paper, it refers to the robust and tunable adjustment of a neuron's firing properties [5]. For example, a neuron can be tuned to perform a given function by expressing in the membrane a specific set conductances with a specific dendritic distribution (Migliore (2003)); degeneracy can result in this tuning being robust, by implementing the same function with many different configurations of the same set of conductances. This property has been systematically studied in crab stomatogastric ganglion neurons [2, 6] and in Globus Pallidus neurons of the rat [7]. In the present study, we investigate this issue for neurons of the hippocampal CA1 region. These neurons are important because they have a critical position as the main output stage of the hippocampal circuitry [8]. The hippocampal CA1 pyramidal neurons, in particular, exhibit a peculiar ensemble and distribution of conductances (reviewed in [9]), subject to significant changes following

activity-dependent biochemical processes, such as activation of protein kinase A and C, or Ca/calmodulin dependent kinase II [10, 11, 12], pathological conditions (e.g. [13, 14]), or traumatic brain injuries [15, 16]. There must then be an extremely robust compensatory mechanism in these neurons, or in the network, which maintains or re-establishes the physiological activity within an operation range, in spite of a potentially large change in its intrinsic properties or synaptic input. Here we study the mechanism of robustness of intrinsic properties by using a unified data-driven workflow and open source analysis and simulation tools. From a set of experimental recordings and morphological reconstructions, we implemented many morphologically and biophysically accurate models for CA1 pyramidal neurons and interneurons, with intrinsic electrophysiological properties constrained by and consistent with the experimental findings. The results indicate that a few currents need to be expressed at a relatively stable level, whereas others can be expressed within a much wider range. The analysis of the model neurons suggests many specific experimentally testable predictions on the combination and relative proportion of the different ionic conductances, and their relationship to robustness of intrinsic properties.

Results

Experimental data used for modeling

To implement a set of data-driven neuron models, we start from a set of morphological reconstructions of neurons and somatic voltage traces obtained from *in vitro* slice preparations of rat hippocampal tissue to use as constraints (see Methods). In Fig 1 we show several examples of the 34 morphologies used in this work (19 pyramidal cells and 15 interneurons), superimposed on a rat hippocampal slice stained for parvalbumin for illustrative purposes.

Fig 1. The 3D reconstructions of CA1 cells in rat hippocampus used in this study.

(Top) ***Pyramidal cells;*** dendrites are shown in black, axons in red; cell identifier**,** from left: 990803, oh140807_A0_idJ, oh140807_A0_idH, oh140807_A0_idG, oh140807_A0_idF, 050921AM2,

oh140807_A0_idC, oh140807_A0_idB, oh140807_A0_idA; (Bottom) ***Interneurons,*** from left to right: basket cell (dendrites in black, axon in pink [Cell number 990111HP2]); bistratified cell (dendrites in black, axon in blue [Cell number 980513B]); axo-axonic cell (dendrites in black, axon in purple [Cell number 970911C]); OLM cell (dendrites in black, axon in dark blue [Cell number 011017HP2]); Ivy cell (dendrites in black; axon in light pink [Cell number 010710HP2]); perforant path associated cell (dendrites in black, axon in red [Cell number 011127HP1]); Schaffer collateral-associated cell (dendrites in black, axon in green [Cell number 990827IN5HP3]). Reconstructions by Joanne Falck and Sigrun Lange. SO Stratum Oriens, SP Stratum Pyramidale, SR Stratum Radiatum, SLM Stratum Lacunosum-Moleculare. 3D reconstructions of the PPA, OLM, axo-axonic cells and of other examples of different types of cells are available in Supplementary figure 1 of Mercer and Thomson [17].

A total number of 1456 experimentally obtained somatic voltage traces for a range of stimulation protocols were used in the optimization pipeline to constrain the models (see Methods). Collections of traces for individual neurons were manually assigned to four electrical types (e-type), according to the firing pattern exhibited during increasing somatic current injections [18], and using the classification proposed in the Petilla convention [19]. The 832 traces from pyramidal neurons, with an increasing inter-spike-interval (ISI), were all classified as continuous accommodating cells (*cAC)*. For interneurons, 240 traces were classified as *cAC*, 160 traces as bursting accommodating cells (*bAC)*, and 224 traces, whose firing rate is constant, as continuous non-accommodating cells (*cNAC)*. Typical examples illustrating the physiological variability observed for these e-types are shown in Fig 2. A more quantitative analysis and comparison of their features will be presented elsewhere (Bologna et al., manuscript in preparation). Different pyramidal neurons (Fig 2, *pyr cAC*) exhibited significantly different responses to the same input. For example, a near-threshold 0.4 nA somatic current injection may or may not generate a few action potentials, whereas a 0.8nA input can result in a 2-fold range for the number of elicited action potentials (APs) (Fig 2, *pyr cAC*, blue traces).

Interneurons classified as *cAC* also exhibited a large inter-cell variability, with different cells responding to the same stimulus with a wide range of spike patterns, such as tonic firing (Figure 2, *int cAC* plots, cell *970428A1*), stuttering (cell *970509HP2*), and depolarization block (cell *980205FHP*). The other two interneuron e-types, *bAC* and *cNAC*, also exhibited a large variability among different cells (Fig 2, *bottom plots*). This variability can be the result of different morphologies and/or a different density and distribution of the conductances expressed on the membrane of the different neurons. In the following sections, we will explore in more detail this issue by implementing and analyzing cellular level models that are able to reproduce these results.

Fig 2. Experimental voltage traces used for the optimization pipeline.
(Top) Typical somatic traces obtained during a step current stimulation protocol (-0.4, 0.4 and 0.8 nA for 400 ms) from intracellular recordings performed using sharp electrodes on CA1 pyramidal cells (left) and interneurons (right) classified as continuous accommodating cells (*cAC*); (bottom) typical traces from interneurons classified as bursting accommodating, *bAC*, (left) and continuous non-accommodating, *cNAC*, (right) cells [18].

Model Optimization

For each e-type (see S1-S4 Tables and *Methods*), a set of electrophysiological features were extracted from all voltage traces belonging to that e-type. All the pyramidal cell morphologies were used to implement *cAC* models, whereas interneuron morphologies were used to obtain *cAC*, *cNAC*, and *bAC* models following the known firing behavior of each type of morphology (see legend of Fig 1 and S5 Table). Features and morphologies were then used to obtain a set of optimized models for each e-type, using a heuristic parameter optimization process that employed multi-objective genetic algorithms. Each optimization run (see *Methods* for details) returned a number of viable "individuals", each one with a specific ensemble of peak ion channel conductance and passive properties consistent with the chosen "objectives" (i.e. a set of experimental features). As a cost

function for the optimization process we used a score defined by the total error associated with each individual, calculated as the sum of the absolute deviations of model features from the experimental mean, in units of the experimental standard deviation (*sd*) obtained for the value of each objective. A score=0 would correspond to an individual with all parameters equal to the average value of the corresponding experimental electrophysiological feature. The total error thus gave an idea of how good the individual was in representing the neuron's overall expected behavior under a series of 400 ms long somatic current injection steps. The final choice to accept an individual as a plausible representation of a given e-type was based on the error obtained for each objective. An individual with a $sd<2$ for all objectives was considered acceptable.

Typical optimization results for pyramidal and interneuron *cAC* e-types are shown in Fig 3. Traces obtained for different somatic current injections from three individuals (Fig 3, traces on top left graph of each panel), showed that the optimization process was able to take into account the experimental variability. Different individuals exhibited significantly different responses to the same stimulus, as in the experiments. The evolution of the total score as a function of the number of generations in the optimization process (bottom graph in each panel), showed that the optimization converged nearly monotonically in relatively few iterations, having reached a relatively stable minimum within approximately 60 generations. The list of objective scores for the best individual in each case (Fig 3 right graph in each panel) showed that for most features (n=60 for pyramidal cells and n= 47 for *cAC* interneurons, see S1-S4 Tables) the associated error was below 2 sd. Similar results were obtained for the optimizations of *bAC* and *cNAC* interneurons (data not shown). Taken together, these results show that the overall optimization process is a robust way to obtain a number of

biophysically accurate neuron models of hippocampal CA1 pyramidal cells and interneurons, which are able to reproduce many of the properties observed experimentally in different types of neurons.

Fig 3. Model optimization.

Typical optimization results for *cAC* pyramidal cells (top) and interneurons (bottom). The top left graph of each panel shows a few examples of model traces from three individuals during a current injection of -0.4, 0.4, and 0.8 nA (black, red, and blue traces, respectively). The right graph of each panel reports the objective scores for the best individual. The bottom left graph in each panel shows a typical evolution of the total score during an optimization run.

A more direct comparison between experimental and modeling traces for the different e-types is shown in Fig 4A, revealing a very good qualitative agreement between the modeling results and experimental traces. The optimization enabled the production of models that correctly reproduced many characteristics of the firing patterns, such as the strong accommodation observed in *cAC* interneurons (Fig 4A, *cAC* int @0.4nA), the high firing frequency of *bAC* interneurons at the beginning of a current injection (Fig 4A, *bAC* @0.6nA), and the progressive reduction in the AP amplitude during the first part of stronger stimuli (Fig 4A, *bAC* @1nA). The pyramidal cell models also exhibited a typical property often observed experimentally in this type of cells, i.e. the decrease in the peak amplitude of an AP backpropagating into the apical dendrites [20]. This effect has been shown to depend on the high density of A-type potassium channel in the apical dendrites [21], but not all CA1 pyramidal neurons exhibit this effect [22, 23]. It is important to note that this feature was not used to constrain the optimization but, interestingly, the optimized models were able to reproduce it, as shown in Fig 4B, for a few cases using morphologies from both young adult (cells 050921AM2, and 990803) and P14-23 animals. The dichotomy in AP backpropagation observed in the experiments [22] was also reproduced by the model neurons, with the AP amplitude either strongly decreasing beyond ~150 μm from the soma or limited to ~50% of the maximum, with very few cases in between.

209 Taken together, this comparison between experiments and models at the individual trace level,
210 suggests that the optimization process was able to correctly capture and explain both intra- and inter-
211 cell variability in firing behavior in terms of different combinations of active and passive membrane
212 properties.
213
214 **Fig 4. Optimization results.**
215 (A) Comparison between typical experimental and model traces for each e-types under different
216 somatic current injection. (B) Peak amplitude of an AP backpropagating in the main apical dendritic
217 trunk of different pyramidal cell models, as a function of the distance from the soma. Each trace refers
218 to a different morphology, as indicated. Abbreviations: *cAC*, continuous accommodating cells; *cAC*,
219 bursting accommodating cells; *cNAC*, continuous non-accommodating cells.
220
221 An indication of how the optimized models may capture the variety of experimental
222 input/output properties can be drawn from Fig 5, where the number of spikes for each e-type was
223 plotted against the somatic current injection, for experimental (blue lines) and modeling traces (red
224 lines). In all cases, experimental traces exhibited a rather large inter-cell variability in the number of
225 spikes elicited by any given input current. It is quite common to see up to a ~5-fold difference in the
226 number of spikes elicited in different cells under the same current injection. In most cases, the models
227 were in quantitative agreement with the average number of spikes generated as a function of the input

current (Fig 5, insets, Mann Whitney Rank Sum test $p>0.05$ in all cases except for 1nA injection in pyramidal neurons).

Fig 5. Input/Output properties.

Number of spikes as a function of the input current from experiments (blue traces) and models (red traces) for the various e-types. The insets show the corresponding average values. Abbreviations as in Fig 4.

Degeneracy within a population

With the set of data-driven neuron models obtained for each e-type, we can now analyze how different combinations of peak conductances can result in models able to reproduce equally well the firing properties observed experimentally under different current injection steps. The optimization process generates many of these models (termed "individuals") because of ion channel degeneracy [5]. As discussed in the *Introduction*, this phenomenon is thought to allow a neuron to adjust its firing properties in a robust and tunable manner.

Fig 6. Degeneracy in CA1 pyramidal neurons.

Optimized values for all parameters, obtained for the 10 best individuals from each optimization. The X-axis represents the individual optimizations (each composed by 10 individuals), the Y-axis is the parameter's name. The pixel colors represent the value of the parameter, normalized to the maximum value obtained from all optimizations of a given e-type. The color scale is shown on the right. Abbreviations as in Fig 4. In all cases the total error was in the range of 29-42 sd.

To obtain further insight into on how degeneracy is achieved in hippocampal CA1 neurons, we analyzed all the individuals obtained from the optimization runs. For each optimization run, the 10 best individuals were considered based on their total score (see Methods). Note that these

individuals were obtained from the same morphology with different channel densities. In Fig 6, the value of the optimized parameters, normalized to the maximum value chosen for each conductance, were plotted for each optimization run (10 individuals for each run, *opt id*). For clarity, in each graph the values obtained for any given parameter were placed on the Y-axis according to the corresponding average value calculated from all optimizations. In this way, the bottom rows in each graph correspond to parameters with an average low value whereas top rows correspond to parameters with higher values. Furthermore, parameters that were relatively stable across all optimizations (i.e. with a sd<0.2) for any given e-type are highlighted using a red label in the y axis. For pyramidal cells (Fig 6, *pyr cAC*) the most stable parameters were some of the passive properties, I_h, K_M, Calcium, and Ca-dependent K currents. Interestingly, we noted that whereas passive properties were consistently optimized with a stable value across the optimizations for all e-types (Fig 6, see top rows in all graphs), conductances were shown to be somewhat different depending on e-types. For example, for interneurons, I_h, somatic K_M and dendritic K_{DR} were the most stable for all e-types, whereas dendritic K_A was stable for *cAC* and Cagk for *cNAC*. These results suggested that each e-type has specific active properties that may be particularly important to obtain the appropriate firing pattern in response to a given input. While these properties need to be well constrained for each e-type, degeneracy can be achieved by combining the other conductances in a relatively large number of ways. The functional consequences of this situation will be discussed below.

To explore whether a cell's morphology can also be related to degeneracy, we fixed the peak conductance values to those found for the best overall individual (obtained for morphology oh140521_B0_Rat_idA) and calculated the total error by using different morphologies. The results are shown in Fig 7A. We found that the total error using the same set of conductances on different morphologies was within the range obtained for each cell's optimization for 10 out of 16 morphologies. For these cases, there was no correlation between the total error and the main morphological properties, such as soma area, total cell volume, or number of sections (Fig 7B, Spearman correlation, $p>0.05$ in all cases). These results suggest that degeneracy can also be obtained

using different morphologies equipped with identical peak channels conductance. A deeper analysis of this issue however was not further considered in this work.

Fig 7. Degeneracy from different morphologies.

(A) (*Black symbols*): the total error calculated from the best individual obtained for each morphology; the dotted line identifies the maximum total error. (*Open symbols*): total error calculated from all morphologies equipped with the set of conductances obtained for oh140521_B0_Rat_idA. (B) Soma area, total cell volume, and number of sections of all morphologies.

For a more detailed analysis of the configuration of peak conductance values for all models, we first considered the results for pyramidal neurons. In Fig 8A we show a typical distribution of normalized values obtained for membrane properties where optimizations yielded a relatively narrow range (somatic K_M, I_h, and Ra), or a wider range of values across individuals (dendritic Na). Note that two of the conductances with a narrow distribution are, in pyramidal CA1 neurons, the dominant factors in controlling major properties such as excitability and accommodation (K_M, reviewed in [24]), and synaptic integration (I_h, [25]). The paramount importance of these two types of conductance for reproducing the experimental traces, suggested by their value lying in a narrow range across individuals, emerged from the optimization process without any specific constraint.

Fig 8. Degeneracy in CA1 pyramidal neurons.

(A) Distribution of the normalized values obtained for the somatic K_M, dendritic Na, I_h and Ra. (B) Radar plot with the values obtained for a subset of conductances. Parameters' values were sorted for those obtained for Cagk (black line); Traces on the left are model traces from individuals #30, 46, 50

303 and 102 under a 0.4 nA somatic current injection. (C) Number of spikes elicited by a 0.4 nA current
304 injection in each individual. Abbreviations as in Fig 4.
305
306 An insight on degeneracy in these neurons can be obtained by considering correlation between
307 parameter pairs. In most cases, we found no statistically significant correlation (see S6 Table for the
308 Spearman correlation coefficients). However, for several cases a significant correlation between
309 selected parameters was found (S6 Table, grey cells). The conductance which was most correlated
310 with others was Cagk, a Ca- and voltage-dependent K^+ conductance that is one of the major
311 determinants for accommodation in these neurons. The inverse correlation with the K_M is particularly
312 interesting, since it supports the experimental finding that these channels operate in combination to
313 control intrinsic hyperexcitability [26], and modeling results suggesting how they must both be
314 involved to obtain a strong accommodation [27, 28].
315 To explore the configuration of the conductances in a more qualitative and intuitive way, we
316 arranged a radar plot of the conductances most correlated with Cagk (Fig 8B), and one of those
317 showing little variability (in this case the reversal potential of the leakage current in the dendrites,
318 e_pas d). The different individuals were sorted with respect to Cagk (Fig 8B, thick black line) and,
319 for clarity, we plotted only 40 of the 160 individuals. The highly jagged and intermixed lines represent
320 the different peak conductance type and value for different individuals giving equally good
321 representations of 60 electrophysiological features experimentally observed in these neurons (see S1
322 Table). Examples of model traces from a few individuals (all obtained with a 0.4nA somatic current
323 injection) displayed the same number of spikes obtained with very different channel configurations.
324 The number of spikes elicited for each individual is plotted in Fig 8C.
325 These results give a clear indication that degeneracy in CA1 pyramidal cells can easily emerge
326 from many different combinations of many, but not all, channels. The reason for the lack of pairwise
327 correlation between most parameters does not exclude that the parameter space may be shaped by

higher order correlations that can be ultimately responsible for degeneracy. However, a full quantitative study of higher order correlations was outside the scope of this study.

The results obtained for interneurons are shown in Fig 9. In this case, to allow an easier comparison of the parameters among the different e-types, individuals were sorted according to the somatic Na conductance (Fig 9, thick black lines), which was among the most correlated with all the others (see Supplementary S7-S9 Tables). The models suggest a few distinct differences among the different e-types. Note, for example, the distribution of values obtained for the peak conductance of dendritic K_{DR} or K_A in the various e-types (Fig 9, dark red and blue lines, respectively), or the difference in the overall values of dendritic Na (Fig 9, orange lines) between *cAC* and *cNAC*. In general, however, the distribution of values were analogous to those obtained for pyramidal cells, with each individual characterized by a highly variable combination of values for many conductances.

Fig 9. Degeneracy in CA1 interneurons.

Radar plot with the values obtained for a subset of conductances. Parameters were sorted for the somatic Na values (black line); the bar graph on the right of each radar plot represents the corresponding spike count from each individual.

Differences in channel proportions among hippocampal CA1 e-types

Finally, one important factor in determining the firing characteristics of different neurons, in addition to a substantial change in morphology [29] and/or gene expression profile [30], is the relative proportion with which specific channels are expressed on the membrane. For this reason, from the optimized models we calculated the relative contribution of each channel in each e-type, by considering the average value of each peak conductance calculated across all individuals. The results are presented in Fig 10A. In all cases, we found that Na, K_A and K_{DR} could account for most of the channels expressed on the membrane. Interestingly, each e-type showed a distinct proportion of these channels, with axonal Na channels playing a relatively large role in all e-types, axonal K_A being

relatively more important in pyramidal neurons than in interneurons, and dendritic K_{DR} being significantly higher in *cNAC* e-types. An analysis of the relative level of each conductance in the various e-types (Fig 10B) also showed significant differences in several cases (Pairwise Multiple Comparison Procedure, $p<0.05$). From the results it is clear, for example, that dendritic Na should be higher in pyramidal cells than in any type of interneuron, *cAC* interneurons should have a higher dendritic Na among interneurons (Fig 10B, dark blue squares for Na d), and that the axonal K_M is essentially independent from cell type. In summary, these results suggest the experimentally testable prediction that different e-types can be characterized by a different combination of the same set of conductances.

Fig 10. Differences among CA1 neuron populations

(A) Pie charts showing for the different e-types the proportion of each conductance with respect to the total average peak conductance calculated across all individuals. (B) Schematic representation of a Pairwise Multiple Comparison Procedure (Dunn's Method), between each pair of e-types. The colored boxes indicate cases for which $p<0.050$. Dark blue or cyan indicates that the average value of the first component is significantly lower or higher, respectively, than the second one. An empty box indicates no statistically significant difference.

Discussion

It has been shown that any individual neuron can express a distinct combination of many channel types [30] determining its electrical properties [31]. Furthermore, several seminal papers demonstrated that each cell type could exhibit specific correlation between channels expression [32], which may emerge from a homeostatic rule [2]. The overall picture is one in which many different conductances coincide to produce the electrophysiological patterns that characterize the operating range of any given population of neurons, and they do so in such a way to compensate for relatively large changes in individual channel density or synaptic connectivity [33]. The robustness of this

mechanism relies on degeneracy [4], which can be practically implemented through a large and flat parameter space for channel conductance. This issue has been studied in the crab pyloric neurons [3], stomatogastric ganglion neurons (e.g. [2, 6]), in the Globus Pallidus neurons of the rat [7]. The presence of degeneracy had yet to be studied in hippocampal neurons. Two recent modeling studies, in the mouse corticospinal neurons and motor cortex, have explicitly shown how degeneracy in cortical neurons can work to implement some electrophysiological features but not others [34], and that degeneracy can also generate multitarget routes from pathological to physiological network dynamics [35]. The first finding was particularly relevant for our study, and it was among the reasons why we choose not to include the voltage between spikes among the optimized features. Its accurate reproduction would have required us to additionally optimize channel kinetics, which was not within the scope of this work.

The analysis of the modeling results presented in this paper provides many experimentally testable predictions on the possible co-regulation of ion currents in hippocampal CA1 neurons. Correlation between pairs of specific conductances has been found for cells in the stomatogastric ganglion of the crab (STG, [32]) and in the pyloric network of the spiny lobster [36]. These experiments found that several pairwise correlations between the same conductances can be present in different type of cells, but no cell type showed conductances with the same set of pairwise correlations. Our optimized models confirmed this result also for the hippocampal CA1 neurons. The models also confirmed pairwise correlations already observed in STG, such as that between K_A and I_h, Na, K_{DR}, and Cagk, and between Na and Cagk. Like in the STG, these correlations were observed in different combinations among different cell types. It is important to stress that the optimization process did not bias the parameter values against each other. Correlations thus emerged naturally from the optimization process, and reflected a better reproduction of the experimental features. The models predict several additional pairwise correlations between conductances (see S6-S9 Tables), which are specific for each e-type. All predictions can be tested experimentally, by directly measuring

405 and comparing peak ion currents or (better) channel densities in different neurons or by a genetic
406 perturbation of channel expression [36, 37].

407 A limitation of this work is that the optimization process was not able to generate a population
408 of models reproducing the very large experimental variability. The reason for this effect is that, in
409 this work, we choose to optimize the different e-types using for each feature the average and standard
410 deviation calculated from all traces, rather than independently optimizing models constrained by
411 traces from an individual cell. A partial explanation for this choice was the limited availability of
412 experimental data on individual cells. Nevertheless, we think that these results offer a significant
413 improvement on the current state of the art, and a necessary step towards building a full-scale cellular
414 model of the rat hippocampus CA1 circuit (Romani et al., in preparation).

415 Another experimentally testable prediction of the models is that each type of cell should have
416 a small number of channel types that would be expressed at the same density in the same neuronal
417 population. There is already some experimental indication that this is the case for STG cells in the
418 crab [1], where it has been found that K_{DR} is relatively constant among the lateral pyloric neurons of
419 different animals, whereas K_A and Cagk varied more than threefold. In this study, we found that
420 passive properties, K_M, and I_h were among the most stable intrinsic membrane properties in any given
421 neuron population, together with dendritic K_{DR} for interneurons.

422 The models also predict that a different combination of axosomatic Na, K_A, and K_{DR} channels
423 may dominate the distribution of channels on the membrane of a neuron belonging to a given e-type.
424 This is also experimentally testable, by directly measuring the density of the different channels
425 expressed on the membrane of different type of neurons.

426 Our analysis suggests a physiological plausible explanation for why single channel mutations
427 can have more or less pathological consequences. A clear example stands out for K_M and I_h channels
428 in pyramidal cells. We found that these channels must be expressed with a relatively stable density;
429 they do not appear to contribute to degeneracy. This may explain why specific mutations of K_M
430 channels can result in neonatal epilepsies in humans [38], or why the decrease in I_h caused by

experimental models for temporal lobe epilepsy can result in major changes in the electrophysiological mechanisms related to cognitive functions [39].

Finally, the modeling effort presented and discussed in this work is part of a larger modeling workflow currently underway in the framework of the EU Human Brain Project (https://www.humanbrainproject.eu/en/), with the main goal to implement a cellular data-driven model of the entire hippocampus. The Hippocampus is a complex brain structure, deeply embedded into the temporal lobe, with a paramount importance for higher brain functions such as learning and memory, and spatial navigation, and is involved in several major brain diseases. In spite of intensive experimental and computational studies, the mechanisms underlying these functions (and dysfunctions) are still poorly understood. A model implementation and analysis at the cellular level may pave the way for a deeper understanding of the diverse and complex functions of this brain region, and of its levels of organization. One of the major steps towards this goal is the implementation of morphologically and biophysically accurate single cell models for the main neuronal populations, equipped with a set of axonal, somatic, and dendritic currents consistent with many experimentally measured electrophysiological features, in such a way as to be able to capture the main I/O properties observed experimentally. Here we have used a general, robust, and flexible tool able to produce, using reasonable computational resources, ensembles of this type of models for CA1 pyramidal cells and interneurons.

Methods

Experimental procedures for interneurons and pyramidal cells 050921AM2, and 990803

Electrophysiology

All procedures used throughout this study were carried out according to the British Home Office regulations with regard to the Animal Scientific Procedures Act 1986. Hippocampal slices were prepared as described previously [40, 41]. Briefly, young adult male rats (Sprague-Dawley, body weight 90–180 g) were deeply anaesthetised with Fluothane (inhalation) and sodium pentobarbitone

457 (Sagatal, 60 mg kg^{-1}, Rhône Mérieux, Harlow, UK) and perfused transcardially with ice-cold
458 modified artificial cerebrospinal fluid) containing in mM: 248 Sucrose, 25.5 $NaHCO_3$, 3.3 KCl, 1.2
459 KH_2PO_4, 1 $MgSO_4$, 2.5 $CaCl_2$, 15 D-Glucose, equilibrated with 95% O_2/5% CO_2. 450 to 500 μm
460 coronal sections were cut (Vibroslice, Camden Instrument, Loughborough, UK) and transferred to an
461 interface recording chamber. They were maintained in modified ACSF solution for 1 hour, and then
462 in standard ASCF (in mM: 124 NaCl, 25.5 $NaHCO_3$, 3.3 KCl, 1.2 KH_2PO_4, 1 $MgSO_4$, 2.5 $CaCl_2$, and
463 15 D-glucose, equilibrated with 95% O_2/5% CO_2) for another hour at 34–36°C before commencing
464 electrophysiological recordings. Intracellular recordings were made using sharp microelectrodes (tip
465 resistance, 90–190 MΩ) filled with 2% biocytin in 2M KMeSO4 under current-clamp (Axoprobe;
466 Molecular Devices, Palo Alto, CA). Current-voltage characteristics of CA1 pyramidal cells and
467 interneurons were obtained from their responses to 400 ms current pulses and recorded with pClamp
468 software (Axon Instruments, USA). Individual neurons were recorded and biocytin-filled for up to 3
469 hours.
470
471 ***Histology***
472 The histological procedures have been described previously [42]. Briefly, the 450-500 μm slices were
473 fixed overnight (4% paraformaldehyde (PFA), 0.2% saturated picric acid solution, 0.025%
474 glutaraldehyde solution in 0.1 M Phosphate buffer). Slices were then washed, gelatin-embedded and
475 50-60 μm sections were cut. Sections were cryoprotected with sucrose, freeze-thawed, incubated first
476 in ABC (Vector laboratories) and then in DAB (3, 3' diaminobenzidine, Sigma) to visualise the
477 biocytin and reveal the morphology of the recorded neurones. Sections were then post-fixed in
478 Osmium Tetroxide, dehydrated, mounted on slides (Durcupan epoxy resin, Sigma) and cured for 48
479 h at 56°C. The calcium-binding protein and peptide content of some interneurons was investigated
480 by immunofluorescence. Sections were cut and permeabilised with sucrose and freeze-thawed. They
481 were then incubated in 1% Sodium Borohydride ($NaBH_4$) for 30 minutes, in 10% normal goat serum
482 for another 30 min and then incubated overnight in a primary antibody solution (mouse monoclonal

anti-Parvalbumin (Sigma) or rabbit polyclonal anti-calbindin (CB) (Baimbridge & Miller, 1982)) made up in ABC solution. Sections were then incubated for 2h in a solution of fluorescently labelled secondary antibodies (anti-mouse fluorescein isothiocyanate (FITC) and/or goat anti-rabbit Texas Red (TR), and Avidin-7-Amino-4-methylcoumarin-3-acetic acid (Avidin-AMCA) made up in PBS). Sections were mounted on slides in Vectashield (Vector laboratories) and studied by fluorescence microscopy. Subsequently, sections were incubated in ABC (Vector laboratories) and then in DAB (3, 3' diaminobenzidine, Sigma) to visualise the biocytin, post-fixed, dehydrated, mounted on slides and cured for 48 h at 56°C. All CA1 neurons were then reconstructed using a Neurolucida software (MBF Bioscience).

Histological procedures for pyramidal cells, except cells 050921AM2, and 990803

For all the other pyramidal cells, *ex-vivo* coronal preparations (300 μm thick) were obtained for the hippocampus of wild type rats (Wistar) brains, post-natal 14– 23 days. The project was approved by the Swiss Cantonal Veterinary Office following its ethical review by the State Committee for Animal Experimentation. All procedures were conducted in conformity with the Swiss Welfare Act and the Swiss National Institutional Guidelines on Animal Experimentation for the ethical use of animals. All *ex-vivo* brain slices were cut in ice-cold aCSF (artificial cerebro-spinal fluid) with low Ca^{2+} and high Mg^{2+}. The intracellular pipette solution contained (in mM) 110 Potassium Gluconate, 10 KCl, 4 ATP-Mg, 10 Phosphocreatine, 0.3 GTP, 10 HEPES and 13 Biocytin, adjusted to 290–300 mOsm/Lt with D-Mannitol (25–35 mM) at pH 7.3. Chemicals were from Sigma Aldrich (Stenheim, Germany) or Merck (Darmstadt, Germany). A few somatic whole cell recordings (not available for this work) were performed with Axopatch 200B amplifiers in current clamp mode at 34 ± 1°C bath temperature. After the recordings, cells were left in whole cell mode for 45mins for biocytin to fill up the cell. The pipette was then carefully removed and the brain slice placed in PFA 4% overnight. Slice were then placed in PBS 1X, biocytin revealing protocol was performed prior to mounting. Reconstruction made by eye with assistance of camera Lucida.

509 ***Computational Methods***

510 The models have been implemented using three-dimensional morphological reconstructions.
511 Electrophysiological features of interest (see next paragraph) were extracted from experimental traces
512 using custom code exploiting the open source Electrophysiological Feature Extraction Library (eFEL,
513 https://github.com/BlueBrain/eFEL). Extracted features were then used for multi-objective model
514 parameter optimizations performed using the open source Blue Brain Python Optimization Library
515 (BluePyOpt, [43]). Both are part of a set of tools integrated into many online use cases of the Brain
516 Simulation Platform (BSP) of the Human Brain Project (https://www.humanbrainproject.eu/en/brain-
517 simulation/). The optimizations were carried out using HPC systems, accessible from the BSP, at
518 either the Neuroscience Gateway (https://www.nsgportal.org/), CINECA (Bologna, Italy), or JSC
519 (Jülich, Germany). On a KNL-based HPC system, a typical optimization run for a pyramidal cell,
520 configured to generate 128 individuals/generation, required approximately 1 hour/generation using
521 128 cores. Typical production runs for each optimization required approximately 60 generations to
522 reach an equilibrated state.

523 The overall optimization approach, of using a genetic algorithm, was similar to other studies
524 (e.g. [35, 44]), but with important qualitative differences: for example, in [35] only one detailed
525 morphology was used, whereas in [44] the authors tested many detailed morphologies but with the
526 soma as the only active compartment. In our case, we used many detailed morphologies and, in all of
527 them, we distributed dendritic conductances constrained by experimental findings. This allowed us,
528 for example, to also reproduce experimental dendritic recordings. We believe that for studying
529 degeneracy of ionic currents in hippocampal pyramidal neurons, known to have active dendrites with
530 fundamental roles in signal integration, our choice can give better results.

531 All experimental and model files will be publicly available upon paper publication, under the
532 BSP Hippocampus model collab (https://collab.humanbrainproject.eu/#/collab/594/nav/5317).
533 Complete model and simulation files will also be available on the ModelDB section of the Senselab
534 suite (https://senselab.med.yale.edu/modeldb/).

Readers interested in running their own optimization can also access the public "Online Use Cases" of the BSP directly related to single cell modeling (https://collab.humanbrainproject.eu/#/collab/1655/nav/28538). A number of tools with an intuitive graphical user interface will guide the user through all steps, from selecting experimental data to constrain the model, to running an optimization to generate a model template and, finally, to exploring the model with *in silico* experiments.

Electrophysiological features

Thousands of electrophysiological features may be used to constrain a model's optimization process and many hundreds of parameters to optimize. Ideally, all of them should be used. In practice, however, this is essentially impossible. The amount of missing information will make the problem ill-defined, and the sheer number of parameters that would be required will result in a substantial overfitting. For this reason, we decided to take into account a selected set of electrophysiological features for each e-type, listed in S1-S4 Tables. They include features that are particularly important in shaping the I/O properties of a neuron, such as the spike count and spike times, and those associated with the resting potential and the input resistance. Their average (±sd) value was calculated from experimental traces, using a custom version of the feature extraction tool.

A total of 225 experimental features were used to constrains the optimization process.

Models configuration

Given the experimentally known differences between pyramidal cells and interneurons, we used different channels' configuration and distribution, as schematically illustrated in S1 Fig. Channel kinetics were based on those used in many previously published papers on hippocampal neurons [45, 46], and validated against a number of experimental findings on CA1 pyramidal neurons. The complete set of active membrane properties included a sodium current (Na), four types of potassium (K_{DR}, K_A, K_M, and K_D), three types of Calcium (CaN, CaL, CaT), the nonspecific I_h current, and two types of Ca-dependent K^+ currents, K_{Ca} and Cagk. A simple Calcium extrusion mechanism, with a

561 single exponential decay of 100 ms, was also included in all compartments containing Calcium
562 channels. In general, channels were uniformly distributed in all dendritic compartments except K_A
563 and I_h, which in pyramidal cells are known to increase with distance from the soma [20, 25]. The
564 values for the peak conductance of each channel were independently optimized in each type of
565 compartment (soma, axon, basal and apical dendrites). The parameters' range, independently for
566 pyramidal cells and interneurons, was defined with preliminary simulations, and it covered a range
567 of at least one order of magnitude.
568

569 **Acknowledgements**

570 We thank the CINECA consortium (Bologna, Italy), the Jülich Supercomputing Centre, and the
571 PRACE association (Partnership for Advanced Computing in Europe), for access to their
572 supercomputer systems. We thank all lab-members who recorded, dye-filled and reconstructed
573 neurones: A. B Ali, A. P. Bannister, R. Begum, J. Deuchars, D. I. Hughes, M. Ilia, J. Kerkhoff, S.
574 Kirchhecker and H. Pawelzik.

References

1. Schulz DJ, Goaillard JM, Marder E. Variable channel expression in identified single and electrically coupled neurons in different animals. Nat Neurosci. 2006; 9(3):356-62. Epub 2006 Jan 29.
2. O'Leary T, Williams AH, Caplan JS, Marder E. Correlations in ion channel expression emerge from homeostatic tuning rules. Proc Natl Acad Sci USA. 2013; 110(28):E2645-54. doi: 10.1073/pnas.1309966110.
3. Zhao S, Golowasch J. Ionic current correlations underlie the global tuning of large numbers of neuronal activity attributes. J Neurosci. 2012; 32(39):13380-8.
4. Edelman GM, Gally JA. Degeneracy and complexity in biological systems. Proc Natl Acad Sci USA. 2001; 98(24):13763-8. Epub 2001 Nov 6. DOI: 10.1073/pnas.231499798.
5. Drion G, O'Leary T, Marder E. Ion channel degeneracy enables robust and tunable neuronal firing rates. Proc Natl Acad Sci USA. 2015; 112(38):E5361-70. doi: 10.1073/pnas.1516400112.
6. Taylor AL, Goaillard JM, Marder E. How multiple conductances determine electrophysiological properties in a multicompartment model. J Neurosci. 2009; 29(17):5573-86. doi: 10.1523/JNEUROSCI.4438-08.2009.
7. Günay C, Edgerton JR, Jaeger D. Channel density distributions explain spiking variability in the globus pallidus: a combined physiology and computer simulation database approach. J Neurosci. 2008; 28(30):7476-91. doi: 10.1523/JNEUROSCI.4198-07.2008.
8. Johnston D, and Amaral DG. "Hippocampus," in The Synaptic Organization of the Brain, Chapter 11, Shepherd GM editor. New York, NY: Oxford Univ. Press, 2003. pp. 417–458. doi: 10.1093/acprof:oso/9780195159561.003.0011.
9. Migliore M, Shepherd GM. Emerging rules for the distributions of active dendritic conductances. Nat Rev Neurosci. 2002; 3(5):362-70.
10. Johnston D, Hoffman DA, Poolos NP. Potassium channels and dendritic function in hippocampal pyramidal neurons. Epilepsia. 2000; 41(8):1072-3. a

11. Johnston D, Hoffman DA, Magee JC, Poolos NP, Watanabe S, Colbert CM, Migliore M. Dendritic potassium channels in hippocampal pyramidal neurons. J Physiol. 2000; 525 Pt 1:75-81. b.
12. Yuan LL, Chen X. Diversity of potassium channels in neuronal dendrites. Prog Neurobiol. 2006; 78(6):374-89. Epub 2006 May 22. Review.
13. Jung S, Warner LN, Pitsch J, Becker AJ, Poolos NP. Rapid loss of dendritic HCN channel expression in hippocampal pyramidal neurons following status epilepticus. J Neurosci. 2011; 31(40):14291-5. doi: 10.1523/JNEUROSCI.1148-11.2011.
14. Wang HL, Xian XH, Song QY, Pang C, Wang JL, Wang MW, Li WB. Age-related alterations of neuronal excitability and voltage-dependent Ca2+ current in a spontaneous mouse model of Alzheimer's disease. Behav Brain Res. 2017; 321:209-213. doi: 10.1016/j.bbr.2017.01.009. Epub 2017 Jan 6.
15. Deng P, Xu ZC. Contribution of Ih to neuronal damage in the hippocampus after traumatic brain injury in rats. J Neurotrauma. 2011; 28(7):1173-83. doi: 10.1089/neu.2010.1683.
16. Lei Z, Deng P, Li J, Xu ZC. Alterations of A-type potassium channels in hippocampal neurons after traumatic brain injury. J Neurotrauma. 2012; 29(2):235-45. doi: 10.1089/neu.2010.1537. Epub 2011 Nov 4.
17. Mercer A, Thomson AM. Cornu Ammonis Regions-Antecedents of Cortical Layers? Front Neuroanat. 2017; 11:83. doi: 10.3389/fnana.2017.00083. eCollection 2017.
18. Markram H et al., Resource Reconstruction and Simulation of Neocortical Microcircuitry. Cell, 2015; 163(2):456–492 DOI: https://doi.org/10.1016/j.cell.2015.09.029.
19. Ascoli GA, Alonso-Nanclares L, Anderson SA, Barrionuevo G, Benavides-Piccione R, Burkhalter A, Buzsáki G, Cauli B, Defelipe J, Fairén A, Feldmeyer D, Fishell G, Fregnac Y, Freund TF, Gardner D, Gardner EP, Goldberg JH, Helmstaedter M, Hestrin S, Karube F, Kisvárday ZF, Lambolez B, Lewis DA, Marin O, Markram H, Muñoz A, Packer A, Petersen CC, Rockland KS, Rossier J, Rudy B, Somogyi P, Staiger JF, Tamas G, Thomson AM, Toledo-

627 Rodriguez M, Wang Y, West DC, Yuste R. Petilla terminology: nomenclature of features of
628 GABAergic interneurons of the cerebral cortex. Nat Rev Neurosci. 2008; 9(7):557-68. doi:
629 10.1038/nrn2402.
630 20. Hoffman DA, Johnston D. Neuromodulation of dendritic action potentials. J Neurophysiol. 1999;
631 81(1):408-11.
632 21. Migliore M, Hoffman DA, Magee JC, Johnston D. Role of an A-type K+ conductance in the back-
633 propagation of action potentials in the dendrites of hippocampal pyramidal neurons. J Comput
634 Neurosci. 1999; 7(1):5-15.
635 22. Golding NL, Kath WL, Spruston N. Dichotomy of action-potential backpropagation in CA1
636 pyramidal neuron dendrites. J Neurophysiol. 2001; 86(6):2998-3010.
637 23. Migliore M, Ferrante M, Ascoli GA. Signal propagation in oblique dendrites of CA1 pyramidal
638 cells. J. Neurophysiol. 2005; 94:4145.
639 24. Marrion NV. Control of M-current. Annu Rev Physiol. 1997; 59:483-504. Review.
640 25. Magee JC. Dendritic Ih normalizes temporal summation in hippocampal CA1 neurons. Nat.
641 Neurosci. 1999; 2:508–514.
642 26. Chen S, Benninger F, Yaari Y. Role of small conductance Ca^{2+} -activated K^{+} channels in
643 controlling CA1 pyramidal cell excitability. J Neurosci. 2014; 34(24):8219-30. doi:
644 10.1523/JNEUROSCI.0936-14.2014.
645 27. Hemond P, Epstein D, Boley A, Migliore M, Ascoli GA, Jaffe DB. Distinct classes of pyramidal
646 cells exhibit mutually exclusive firing patterns in hippocampal area CA3b. Hippocampus. 2008;
647 18(4):411-24. doi: 10.1002/hipo.20404.
648 28. Migliore M, Jaffe DB, Ascoli GA. Hippocampal Microcircuits, ch.12, Springer Series in
649 Computational Neuroscience, ISBN 978-1-4419-0995-4 (2010).
650 29. Mainen ZF, Sejnowski TJ. Influence of dendritic structure on firing pattern in model neocortiCaL
651 neurons. Nature. 1996; 382(6589):363-6.

30. Toledo-Rodriguez M, Blumenfeld B, Wu C, Luo J, Attali B, Goodman P, Markram H. Correlation maps allow neuronal electrical properties to be predicted from single-cell gene expression profiles in rat neocortex. Cereb Cortex. 2004; 14(12):1310-27. Epub 2004 Jun 10.

31. Khazen G, Hill SL, Schürmann F, Markram H. Combinatorial expression rules of ion channel genes in juvenile rat (Rattus norvegicus) neocortical neurons. PLoS One. 2012; 7(4):e34786. doi: 10.1371/journal.pone.0034786. Epub 2012 Apr 11.

32. Schulz DJ, Goaillard JM, Marder EE. Quantitative expression profiling of identified neurons reveals cell-specific constraints on highly variable levels of gene expression. Proc Natl Acad Sci USA. 2007; 104(32):13187-91. Epub 2007 Jul 25.

33. Marder E, Goaillard JM. Variability, compensation and homeostasis in neuron and network function. Nat Rev Neurosci. 2006; 7(7):563-74. Review.

34. Neymotin SA, Suter BA, Dura-Bernal S, Shepherd GMG, Migliore M, Lytton WW. Optimizing computer model of corticospinal neurons to replicate in vitro dynamics. J Neurophysiol. 2017; 117:148-162. doi: 10.1152/jn.00570.2016.

35. Neymotin SA, Dura-Bernal S, Lakatos P, Sanger TD, Lytton WW. Multitarget multiscale simulation for pharmacological treatment of dystonia in motor cortex. Front Pharmacol. 2016; 7:157. doi: 10.3389/fphar.2016.00157

36. MacLean JN, Zhang Y, Goeritz ML, Casey R, Oliva R, Guckenheimer J, Harris-Warrick RM. Activity-independent coregulation of IA and Ih in rhythmically active neurons. J. Neurophysiol. 2005; 94:3601–3617.

37. Cao XJ, Oertel D. Genetic perturbations suggest a role of the resting potential in regulating the expression of the ion channels of the KCNA and HCN families in octopus cells of the ventral cochlear nucleus. Hear Res. 2017; 345:57-68. doi: 10.1016/j.heares.2017.01.001. Epub 2017 Jan 5.

38. Miceli F, Soldovieri MV, Ambrosino P, Barrese V, Migliore M, Cilio MR, Taglialatela M. Genotype-phenotype correlations in neonatal epilepsies caused by mutations in the voltage sensor

of K(v)7.2 potassium channel subunits. Proc Natl Acad Sci USA. 2013; 110(11):4386-91. doi: 10.1073/pnas.1216867110. Epub 2013 Feb 25.

39. Marcelin B, Chauvière L, Becker A, Migliore M, Esclapez M, Bernard C. h channel-dependent deficit of theta oscillation resonance and phase shift in temporal lobe epilepsy. Neurobiol Dis. 2009; 33(3):436-47. doi: 10.1016/j.nbd.2008.11.019. Epub 2008 Dec 16.

40. Pawelzik H, Bannister A P, Deuchars J, Ilia M, Thomson A M. Modulation of bistratified cell IPSPs and basket cell IPSPs by pentobarbitone sodium, diazepam and Zn2+: dual recordings in slices of adult rat hippocampus. Eur. J. Neurosci. 1999; 11:3552–3564. doi: 10.1046/j.1460-9568.1999.00772.x

41. Thomson AM, Bannister AP, Hughes DI & Pawelzik H. Differential sensitivity to Zolpidem of IPSPs activated by morphologically identified CA1 interneurones in slices of rat hippocampus. Eur J Neurosci. 2000; 12: 425–436. DOI: 10.1046/j.1460-9568.2000.00915.x.

42. Hughes DI, Bannister AP, Pawelzik H, Thomson AM. Double immunofluorescence, peroxidase labelling and ultrastructural analysis of interneurones following prolonged electrophysiological recordings in vitro. J. of Neurosci. Methods. 2000; 101(2): 107-116. doi:http://dx.doi.org/10.1016/S0165-0270(00)00254-5.

43. Van Geit W, Gevaert M, Chindemi G, Rössert C, Courcol J-D, Muller EB, Schürmann F, Segev I and Markram H. BluePyOpt: Leveraging Open Source Software and Cloud Infrastructure to Optimise Model Parameters in Neuroscience. Front. Neuroinform. 2016; 10:17. doi: 10.3389/fninf.2016.00017

44. Gouwens NW, Berg J, Feng D, Sorensen SA, Zeng H, Hawrylycz MJ, Koch C, Arkhipov A. Systematic generation of biophysically detailed models for diverse cortical neuron types. Nature Communications 2018; 9:710.

45. Ascoli GA, Gasparini S, Medinilla V, Migliore M. Local control of postinhibitory rebound spiking in CA1 pyramidal neuron dendrites. J Neurosci. 2010; 30(18):6434-42. doi: 10.1523/JNEUROSCI.4066-09.2010.

46. Morse TM, Carnevale NT, Mutalik PG, Migliore M, Shepherd GM. Abnormal Excitability of Oblique Dendrites Implicated in Early Alzheimer's: A Computational Study. Front Neural Circuits. 2010; 4. pii: 16. doi: 10.3389/fncir.2010.00016. eCollection 2010.

Figure S1: CA1 pyramidal neuron and interneuron active properties. Morphologies of a pyramidal neuron (*left*) and an interneuron (*right*), with a schematic indication of channels' distribution on the soma, axon, and dendrites.

Table S1: Electrophysiological features used for optimization of pyramidal neurons

Table S2: Electrophysiological features used for optimization of int *cAC* cells

Table S3: Electrophysiological features used for optimization of int *bAC* cells

Table S4: Electrophysiological features used for optimization of int *cNAC* cells

Table S5: Morphological classes and e-types of the optimized pyramidal cells (*left*) and interneurons (*right*).

Table S6: Spearman correlation coefficient between peak conductance values from pyramidal cell models. Only conductances with at least one significant correlation coefficient >|0.25| (gray cells) are shown. The *p* value corresponding to each coefficient is indicated in italics.

Table S7: Spearman correlation coefficient between peak conductance values from cNAC interneuron models. Only conductances with at least one significant correlation coefficient >|0.25| (gray cells) are shown. The *p* value corresponding to each coefficient is indicated in italics.

Table S8: Spearman correlation coefficient between peak conductance values from bAC interneuron models. Only conductances with at least one significant correlation coefficient >|0.25| (gray cells) are shown. The *p* value corresponding to each coefficient is indicated in italics.

Table S9: Spearman correlation coefficient between peak conductance values from cAC interneuron models. Only conductances with at least one significant correlation coefficient >|0.25| (gray cells) are shown. The *p* value corresponding to each coefficient is indicated in italics.

Figure 1 revised

Click here to download Figure fig1.tif

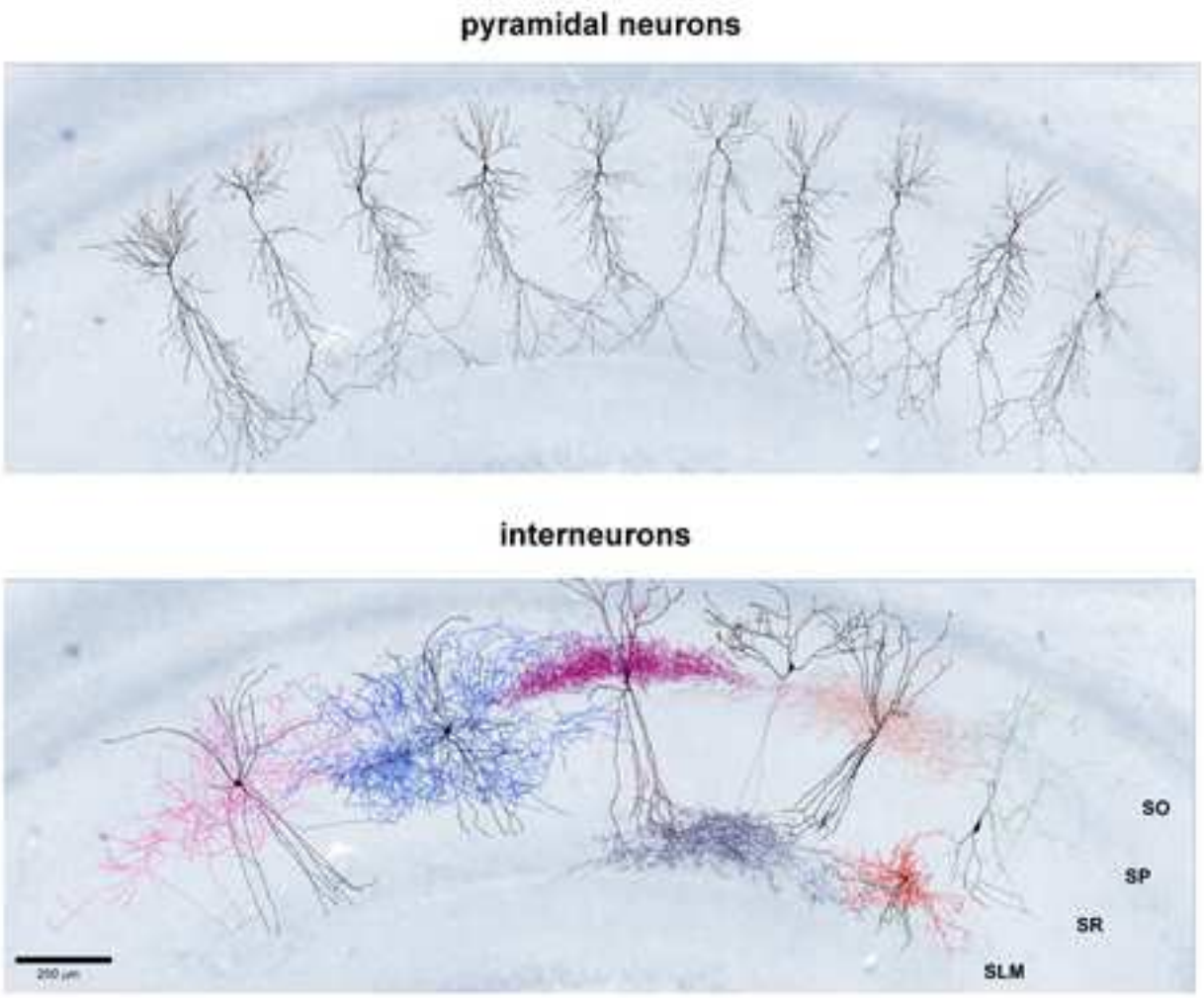

Figure 2 revised

Click here to download Figure fig2.tif

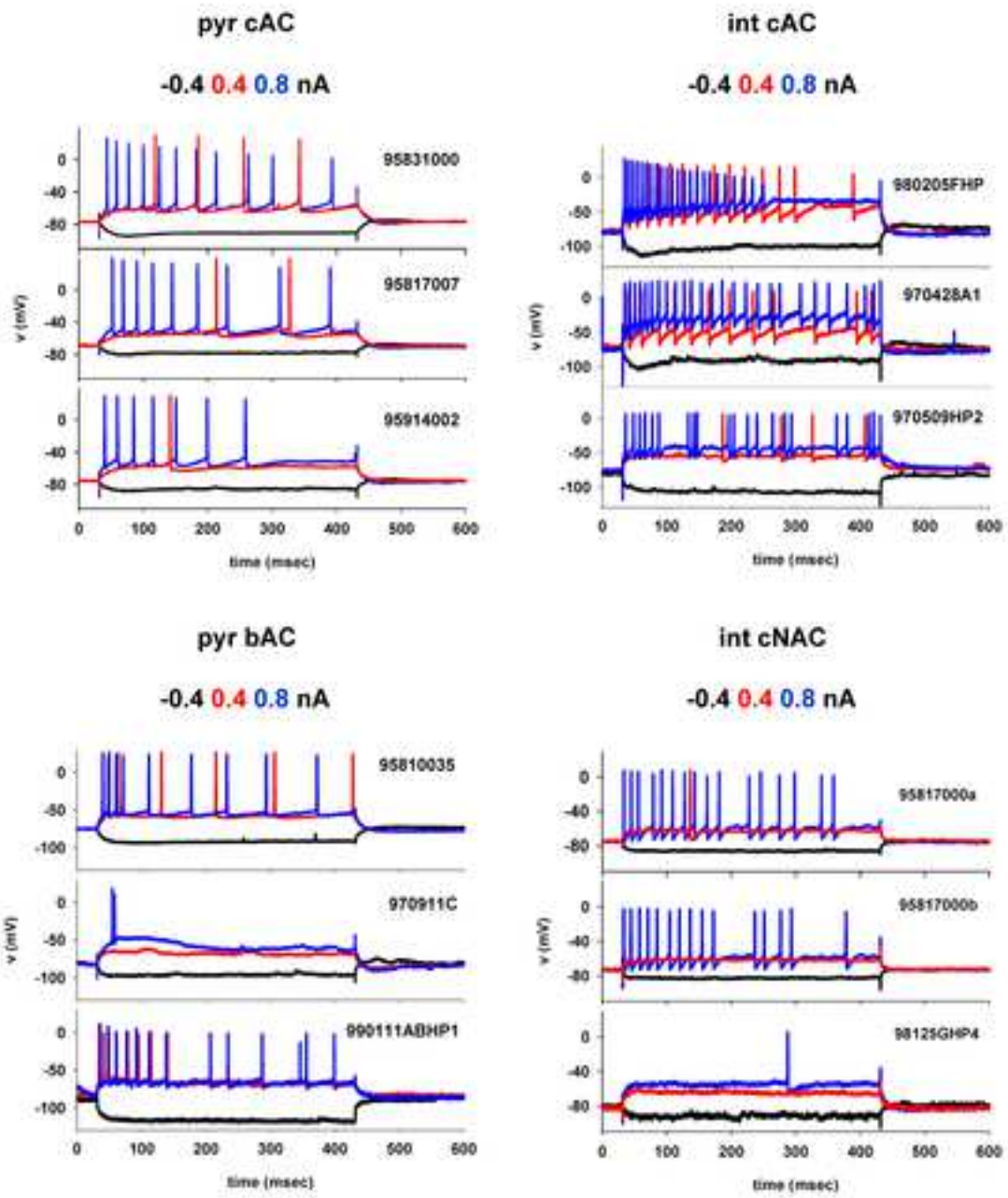

Figure 3 revised

Click here to download Figure fig3.tif

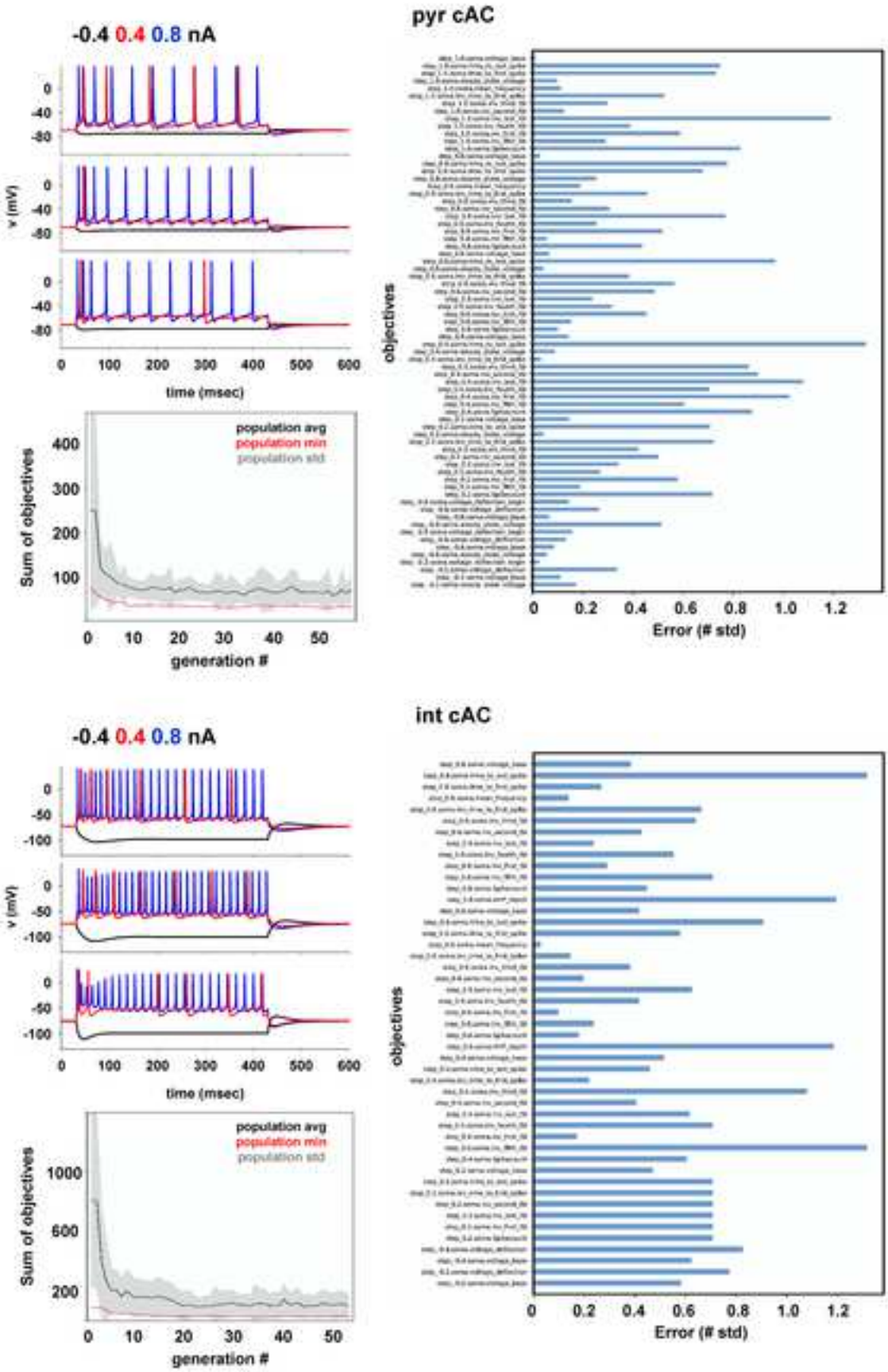

Figure 4 revised

Click here to download Figure fig4.tif

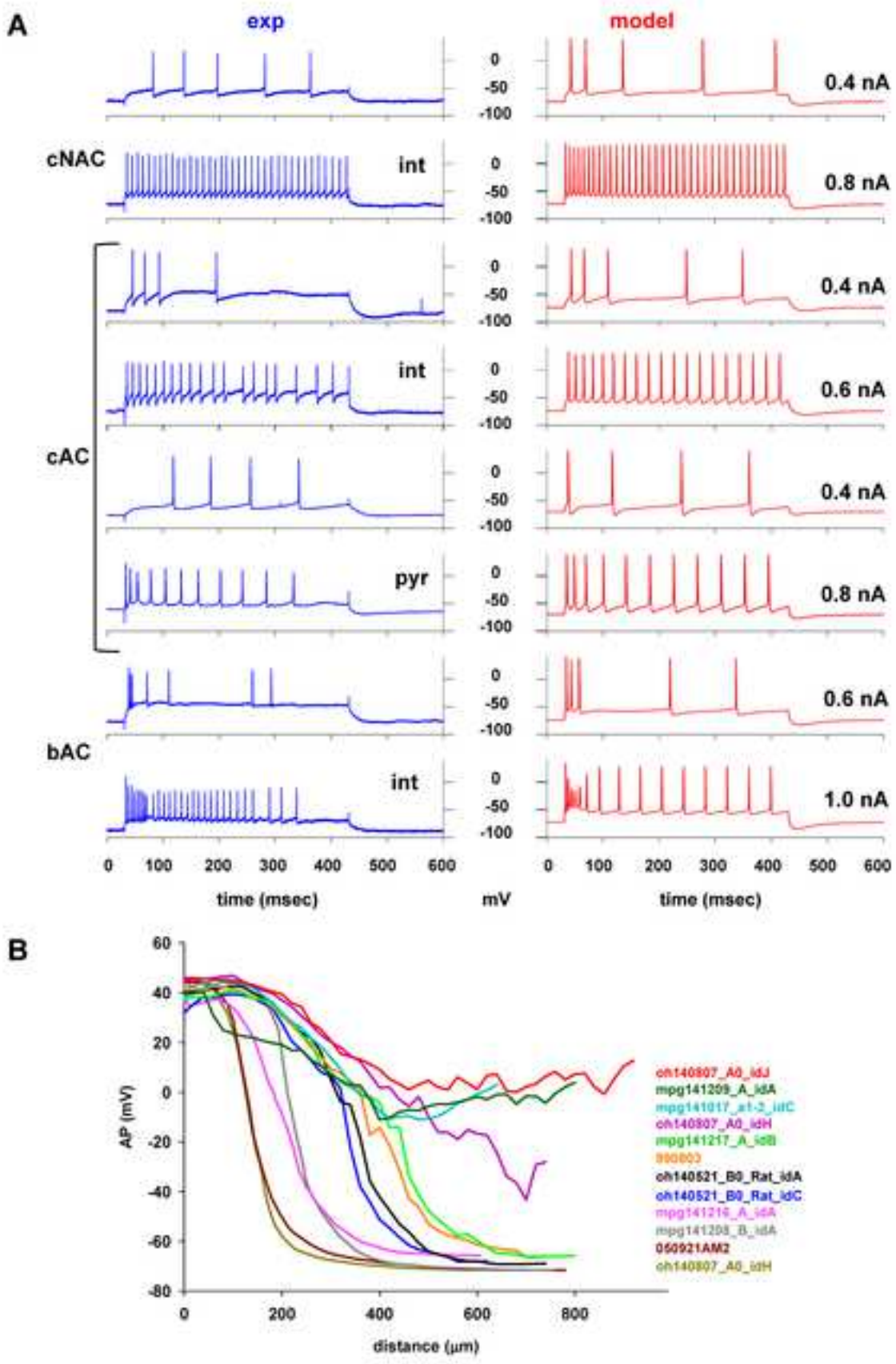

Figure 5 revised

Click here to download Figure Fig5.tif

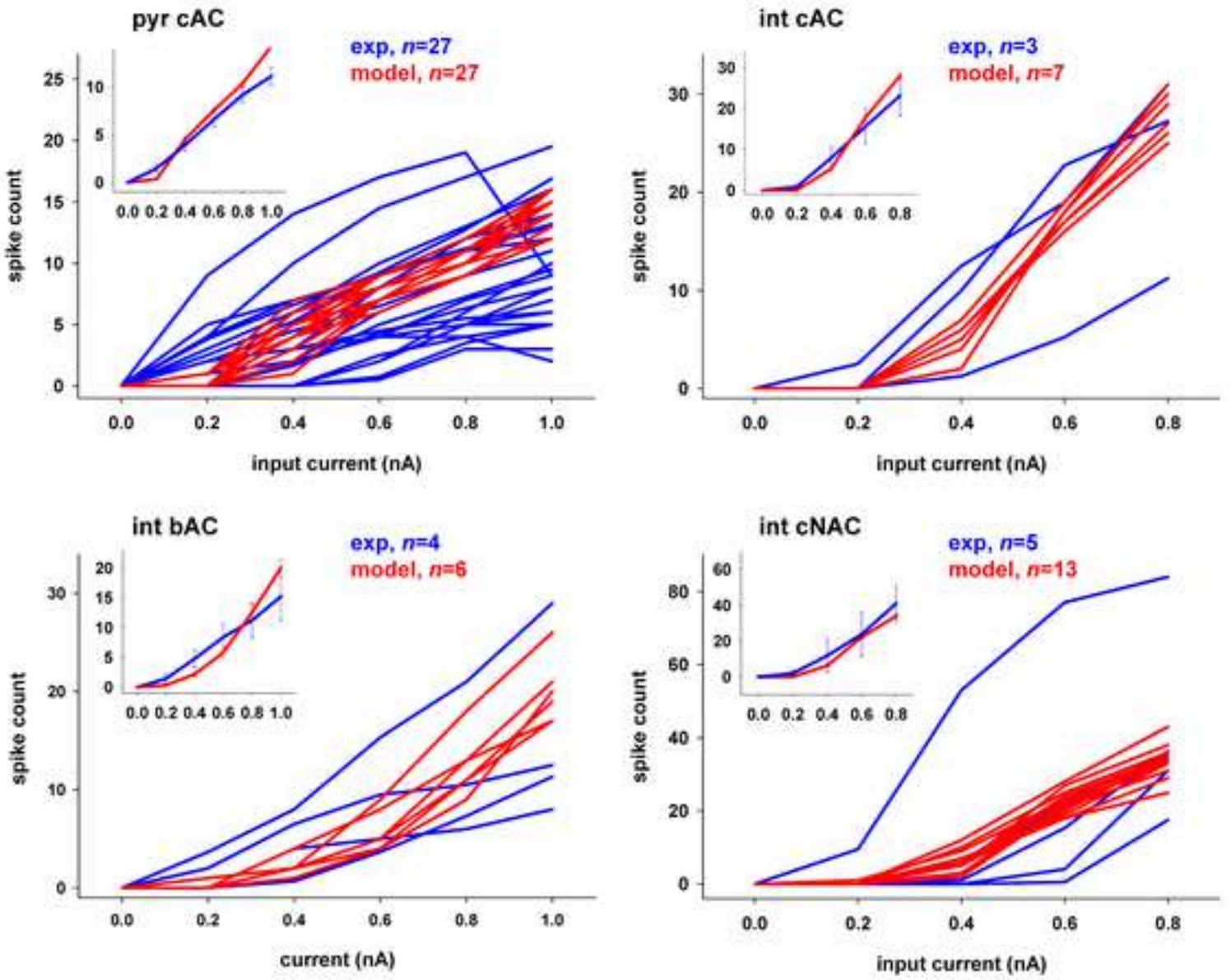

Figure 6 revised

Click here to download Figure fig6.tif

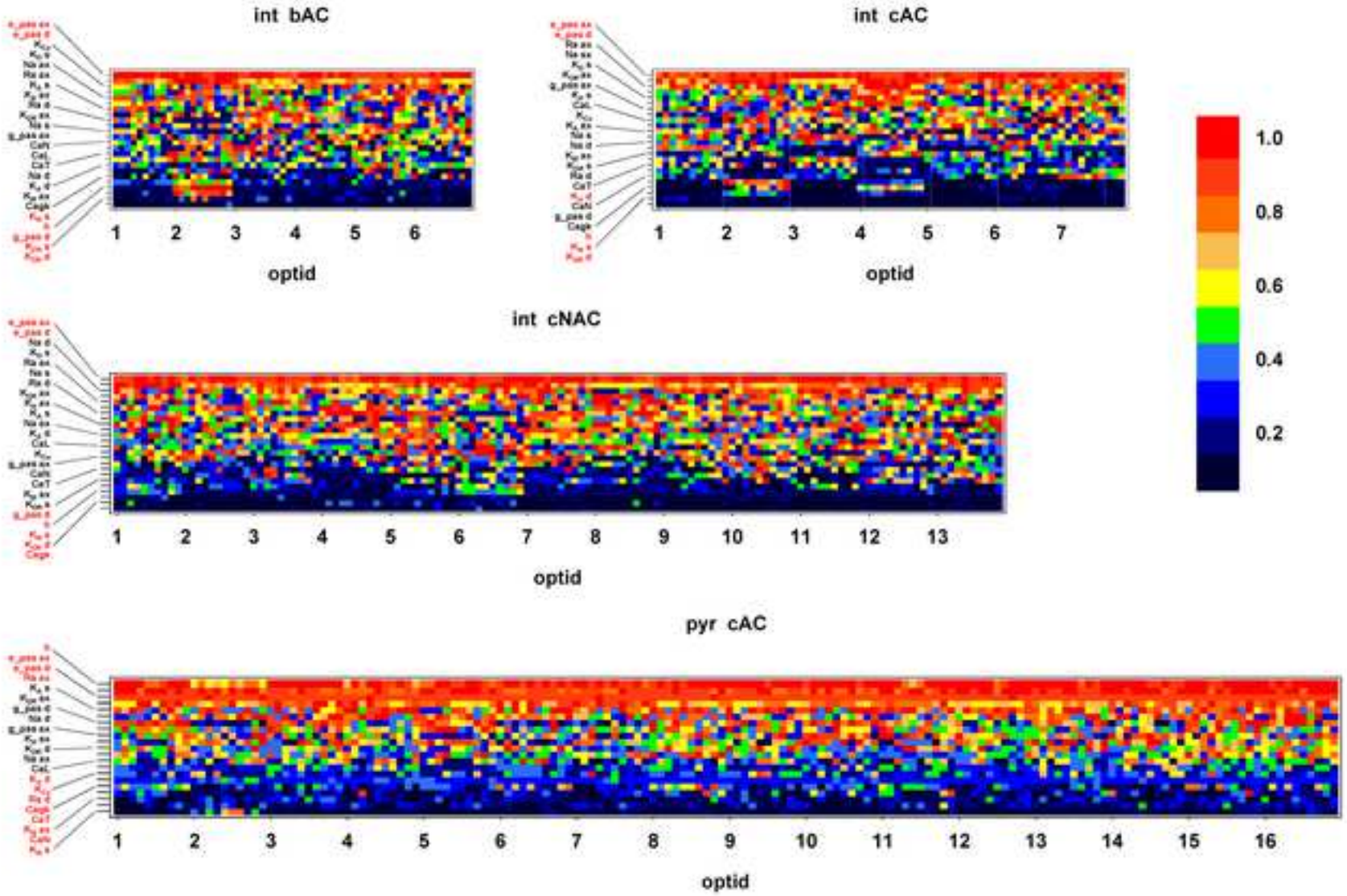

Figure 7 revised

Click here to download Figure fig7.tif

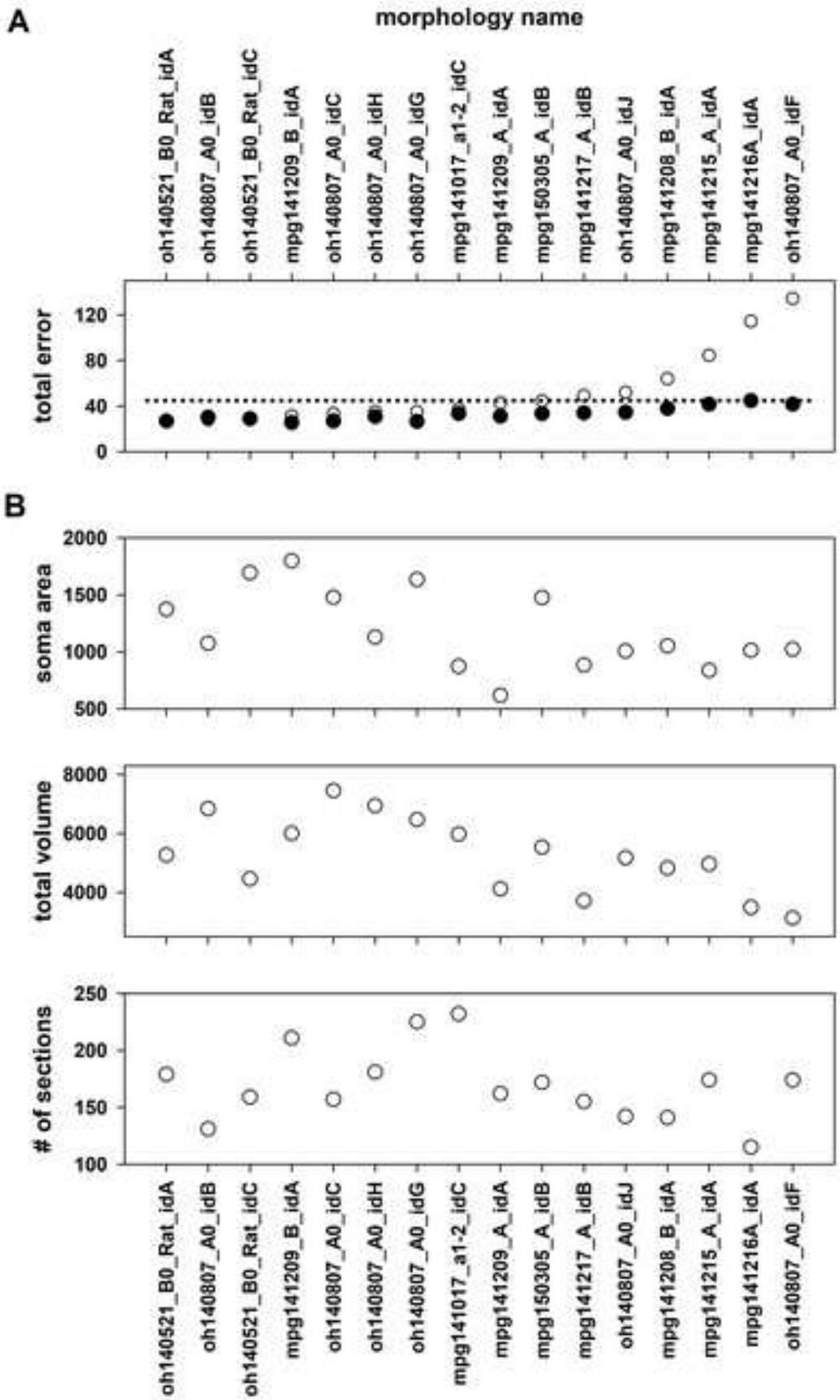

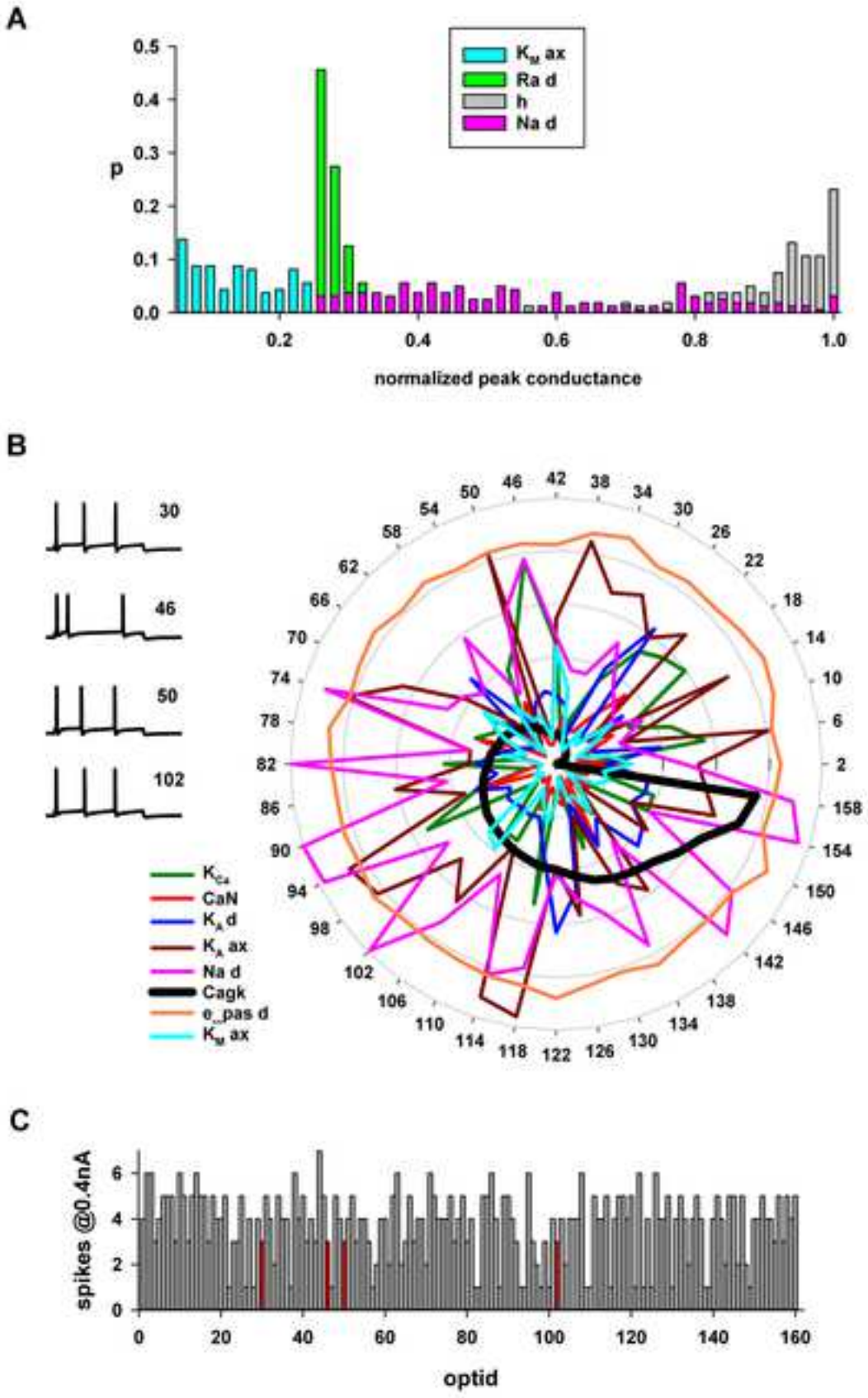

Figure 9 revised

Click here to download Figure fig9.tif

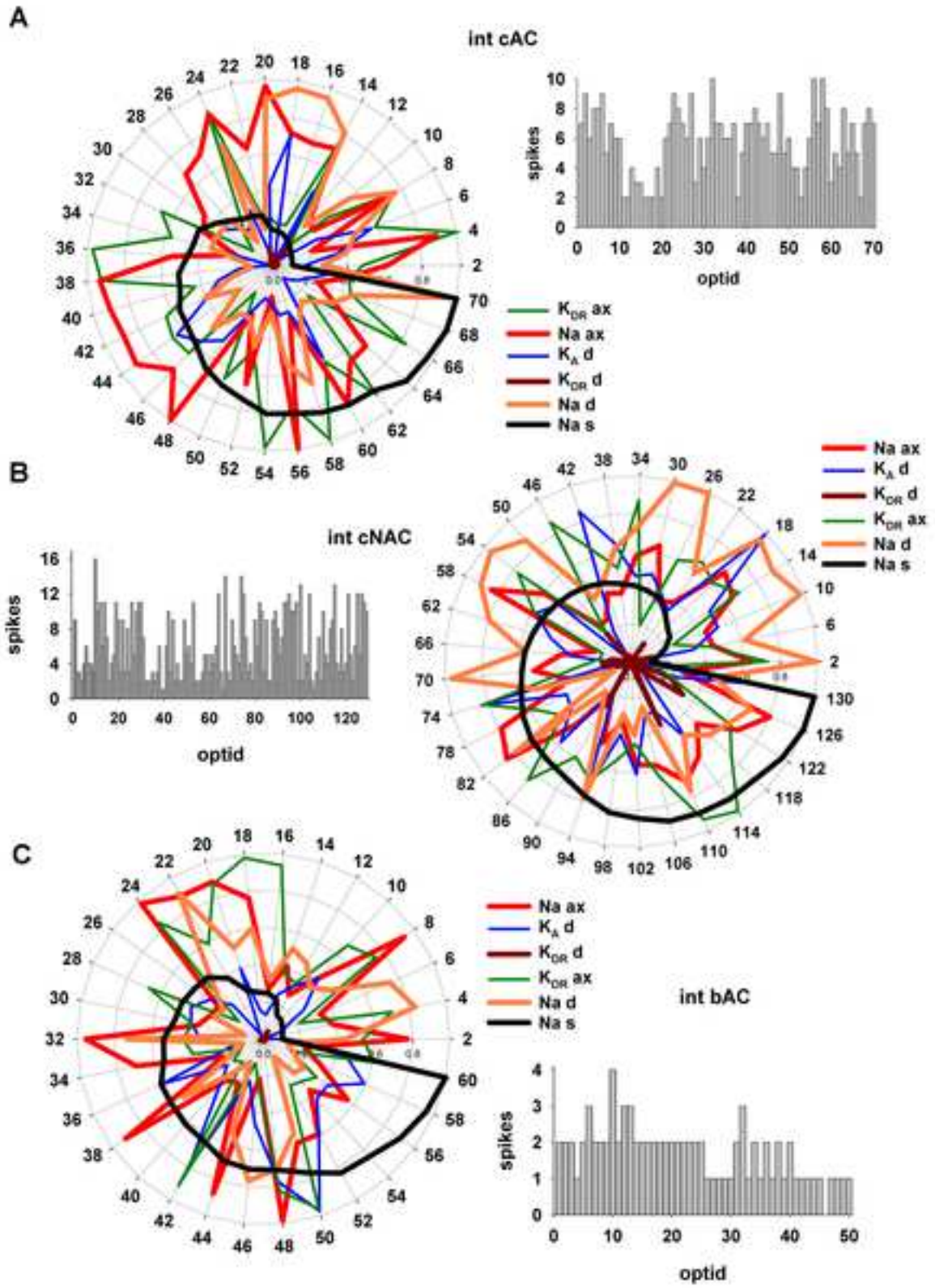

Figure 10 revised

Click here to download Figure fig10.tif

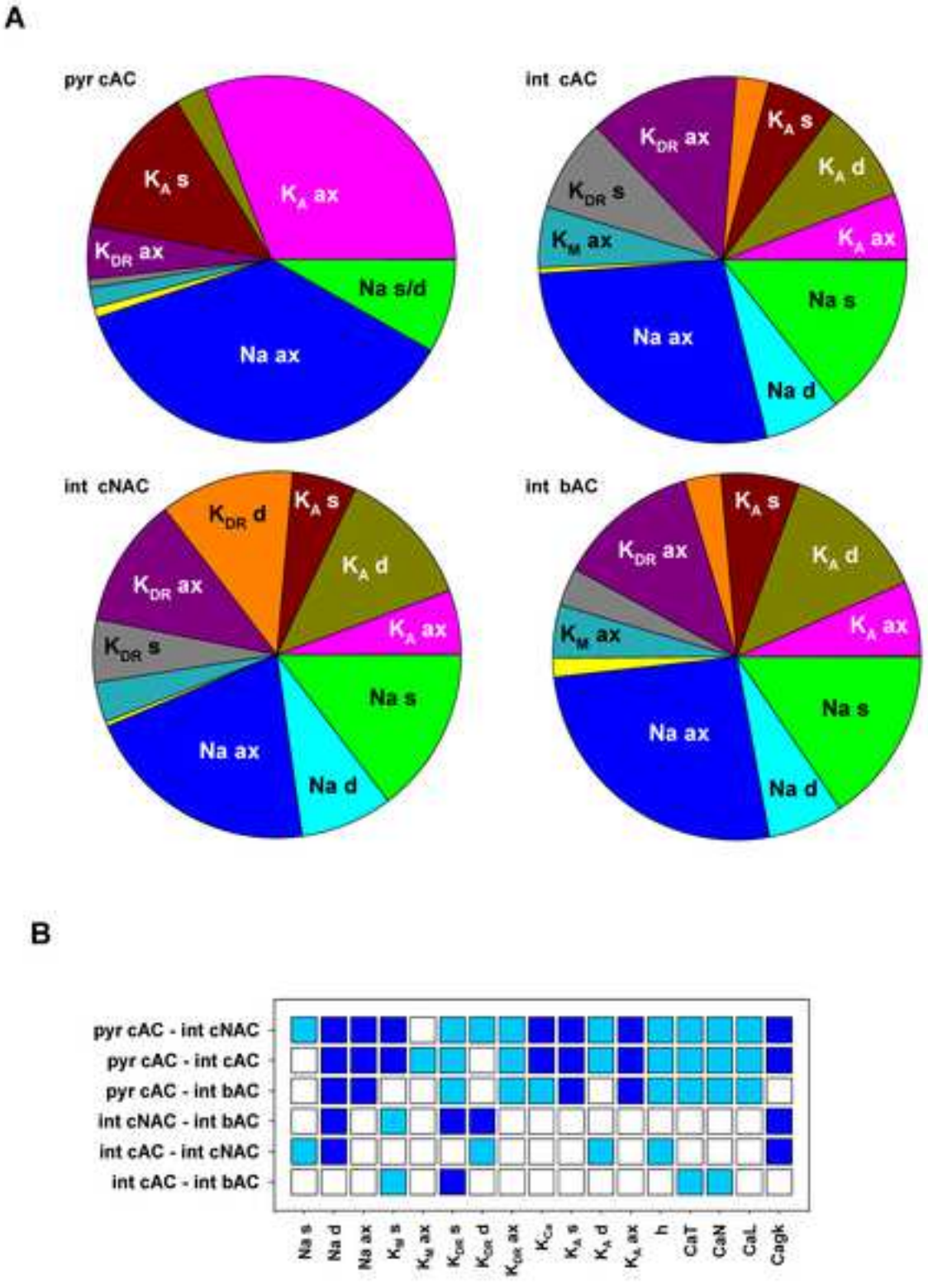

Supporting Information fig S1

Supporting Information Table S1

Click here to access/download

Supporting Information

TableS1.docx

Supporting Information Table S2

Supporting Information Table S3

Supporting Information Table S5